university of groningen / faculty of science and engineering

An analysis of the Standard Model prediction for $\mathcal{B}(B_c^+ \to \tau^+\nu_\tau)$

Bachelor Thesis Physics

Franca Maat (s4280547)

Life, Science and Technology

University of Groningen, the Netherlands

Examiner 1: dr. K.A.M. De Bruyn

Examiner 2: prof. dr. D. Roest

November 11, 2022

Abstract

The currently available numerical Standard Model predictions for the branching fraction of the $B_c^+ \to \tau^+\nu_\tau$ decay are analyzed based on their input parameters. Through error analysis of these parameters, the B_c^+ meson decay constant and the V_{cb} CKM matrix element emerge to be key factors. The study of the B_c^+ meson decay constant prompts an analysis of HISQ and NRQCD formulation used to discretize the heavy bottom quark onto a lattice for lattice QCD calculations. The study of the V_{cb} matrix element prompts an analysis of the different methods of exclusive determinations and another look at the difference between exclusive and inclusive determinations. Based on the obtained insights from these analyses, both an exclusive and an inclusive updated prediction of the branching fraction are computed. The updated prediction of the branching fraction is determined to be $(1.96 \pm 0.09) \times 10^{-2}$ using an exclusive determination of V_{cb} and $(2.28 \pm 0.10) \times 10^{-2}$ using an inclusive determination of V_{cb}. These improved predictions can be used as reference for future comparison to an experimental measurement of this branching fraction, aiding in the search for physics beyond the Standard Model.

Contents

1 Acknowledgements

I started this project with little physics background, but with a lot of motivation. This project was my first experience in particle physics research, which therefore makes me even more grateful that Kristof and Mick gave me this opportunity.
During these months, I have enjoyed all the discussions and all the enthusiasm of everyone at the Van Swinderen Institute. This made me even more enthusiastic about physics.

Andrej, thank you for always being there to explain all my questions, which sometimes were all over the place. From the start of my project, you were the biggest help ever to get me going in particle physics (and physics in general!). Thanks to you, I immediately felt at home and I enjoyed being at the VSI every day. I will miss us chatting about literally anything. I hope your project will go well (which I trust will go great whilst sitting on that fabulous chair that you will take over) and that we can keep in touch.
Mick, thank you for letting me join your office, which made it really cosy when all three of us were there. More seriously however, I want to thank you for always looking out for me.
Finally, Kristof, thank you for being my supervisor and helping me throughout my project. The advice you gave was always exactly what I needed and has therefore helped me to improve on my project a lot. Your clear and patient explanations helped me a great deal and most of all you were always very supportive.

2 Introduction

The first aspect of particle physics that most people encounter is the concept of quarks, which are the smallest particles known. There are six different quark flavors: up, down, charm, strange, top and bottom. These quarks are part of a class of elementary particles called fermions. This fermion class furthermore includes leptons. The lepton family includes the well-known electron and two other charged particles called muon and tau and their respective neutrinos.

The Standard Model (SM) has been very successful in explaining the behaviour of elementary particles. Nonetheless, the SM is not the perfect theory. First of all, the SM is an incomplete theory since it only describes three out of four fundamental forces, omitting the gravitational force. Furthermore, there are some phenomena that cannot be explained by the SM, for example the abundance of matter over antimatter in the universe. The SM predicts that matter and antimatter should have been created in almost equal amounts, which is contradicted by observations of a big asymmetry between matter and antimatter. Another phenomenon that cannot be explained by the current SM is the existence of dark matter and dark energy, which are thought to make up most of the contents of our universe. These quantities are invisible since all light seems to pass through it, as it does not interact with the electromagnetic force. Its presence can only be inferred from gravitational effects. Dark matter and dark energy dominate the structure and evolution of our universe and are therefore important for understanding our universe. [1–3]

These deficiencies of the SM prompt particle physicists to search for physics beyond the Standard Model (BSM). At the time of writing, no conclusive evidence has been found of BSM. Nonetheless, numerous hints of BSM have been found which further encourage the search for BSM. This search can be performed by comparing experimental results to their respective SM theoretical prediction. An example of one of these searches for BSM, relevant for this thesis, is testing for lepton flavour universality (LFU). LFU follows from the SM since the SM describes the three charged leptons as identical apart from a difference in their mass. Therefore, the charged leptons are expected to couple in an identical way to their respective interaction particles, which means that lepton flavor has no effect on the coupling between charged leptons and bosons. LFU violation would be a clear sign of BSM. Therefore, examining LFU is a good test of the SM. [4]

This LFU can be tested for using the Large Hadron Collider beauty (LHCb) experiment. Their LHCb detector specifically focuses on measuring bottom quark decays. The plan of the LHCb group at the Van Swinderen Institute is to experimentally measure the tauonic decay of the B_c particle, containing a bottom and a charm quark. This decay, $B_c^+ \to \tau^+\nu_\tau$, will be measured using the data that the LHCb experiment at CERN will collect in the following years. In the $B_c^+ \to \tau^+\nu_\tau$ decay mode, the B_c meson decays into a final state containing only leptons, specifically a charged tau lepton and a tau neutrino. This decay is a probe for LFU violation since it can be compared with decay modes to the other leptons, $B_c^+ \to \ell^+\nu_\ell$. This comparison can be made between the branching fraction, the probability of the decay mode, of the tauonic decay and branching fraction of the decay modes to the other leptons, which produces a ratio. This experimental ratio can in turn be compared with the SM expectation of this ratio. Experimental results of ratios of equivalent decays have been shown to deviate from the SM expectation [5]. Since the decay mode $B_c^+ \to \tau^+\nu_\tau$ has not been measured before, it could provide new information in the search for BSM.

To be able to make this comparison using $B_c^+ \to \tau^+\nu_\tau$, the SM prediction for the branching fraction of the tauonic decay $B_c^+ \to \tau^+\nu_\tau$ should be as accurately as possible. The branching fraction for $B_c^+ \to \tau^+\nu_\tau$ decay within the Standard Model is about 0,02 [6, 7]. The currently available predictions differ by a factor 2 in uncertainty, which brings up the question where this difference comes from and how this difference effects the branching fraction prediction. This will be investigated by analyzing the involved input parameters, which will reveal their underlying controversies and lead to an updated prediction of the branching fraction.

3 The Standard Model and its elementary particles

Matter is composed of elementary particles. These elementary particles can be divided into particles with a half-integer spin called fermions and force carriers with an integer spin called bosons. This division can also be observed in figure 1, where the mass, charge and spin of each known elementary particle is given and a division is made based on these properties.

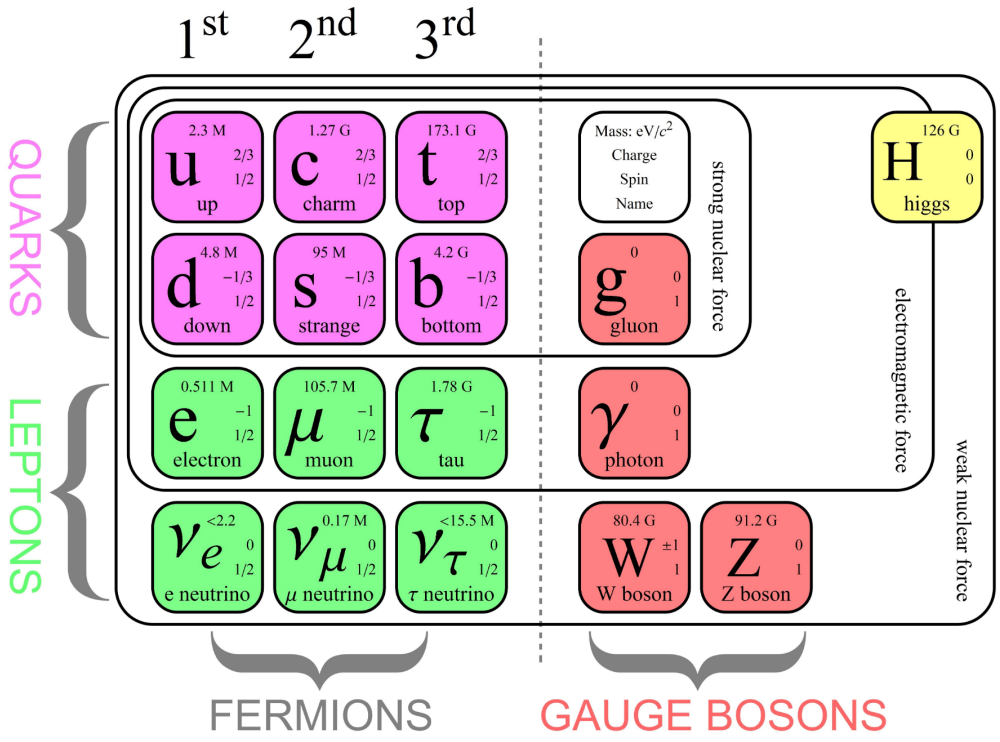

Figure 1: The Standard Model of particle physics. [8]

3.1 Fundamental forces and bosons

Interactions between elementary particles are governed by four fundamental forces, mediated by boson force carriers. These boson force carriers can be observed at the right side of figure 1.
The strongest of the fundamental forces is the strong nuclear force. It uses gluons as force carriers to interact over short distances of about 10^{-15} meters. The second of four fundamental forces is the electromagnetic force. This force is weaker than the strong nuclear force, but acts over infinite distances using photons as their force carriers. Both the bosons of the strong nuclear force and the bosons of the electromagnetic force, gluons and photons, are massless. The weak nuclear force is an even weaker fundamental force than the electromagnetic force and acts over short distances of about 10^{-18} meters. This weak force is mediated by W^+, W^- and Z bosons, which have a mass of 80.4 and 91.2 GeV respectively. The last of the four fundamental forces, the gravitational force, can act over infinitely large distances and is by far the weakest force. This gravitational force could possibly be mediated by bosons called gravitons, but these have not yet been discovered. [2, 9]

3.2 Fermions

Fermions can be sub-divided into quarks and leptons, as can be observed in figure 1. Leptons are fermions that cannot interact via the strong nuclear force, while quarks can interact via the strong force. Leptons can be subdivided into -1e charged leptons and neutral neutrinos. Quarks can be subdivided into up-type quarks with a charge of $+\frac{2}{3}e$ and down-type quarks with a charge of $-\frac{1}{3}e$.
Both quarks and leptons can be organized into three generations with increasing mass, which was proposed by Kobayashi and Maskawa in 1973 [10]. Each generation contains an up-type quark, a down-type quark, a charged lepton and a neutral neutrino as can be observed in figure 1. The first generation

contains the up quark, down quark, electron and electron neutrino. Similarly, the second generation contains the charm quark, strange quark, muon and muon neutrino. Finally, the third generation contains the top quark, bottom quark, tau and tau neutrino.

An important characteristic of quarks is that they have a property called 'color' allocated to them. Any quark can exist in three different color states, which are indicated as the colors red, green and blue for convenience. Isolated particles must be color neutral according to the theory of color confinement [2]. This means that isolated quarks cannot be observed, since quarks are not color neutral. Therefore, quarks organize themselves into composite particles, called hadrons. Hadrons are simply particles in which two or more quarks are grouped together. There are several types of hadrons of which mesons and baryons are the most important examples.
A meson consists of one quark and one anti-quark grouped together. The quark has a specific color and the anti-quark must have the respective anti-color, to render the meson color neutral. Mesons that are made of a pair of quark and anti-quark of different flavor are called flavored mesons. The names of flavored mesons are dependent on the heavier quark, for example flavored mesons with the heaviest quark being a bottom quark are named B-mesons and flavored mesons with the heaviest quark being a strange quark are named kaons.
A baryon consists of three quarks grouped together. All three quarks in the baryon must have a different color for the baryon to be color neutral. Examples of a baryon are protons, containing two up-quarks and one down-quark, and neutrons, containing one up-quark and two down-quarks. [11]

This thesis is about a particle called a B_c meson, which contains a bottom (anti-)quark and a charm (anti-)quark. When the meson contains a charm quark and a bottom anti-quark, it is a B_c^+ meson since its charge is calculated as $\frac{2}{3}e - -\frac{1}{3}e = 1$. On the other hand, when the meson contains a charm anti-quark and a bottom quark, it is a B_c^- meson since its charge is calculated as $-\frac{2}{3}e - \frac{1}{3}e = -1$. [2]

3.3 Decay of the B_c meson

The SM decays of particles can be described by equations and visualized using Feynman diagrams, which are space-time diagrams that describe how particles move and interact. [9]
In Feynman diagrams, all particles can also be replaced by their antiparticles and the decay is still allowed, therefore the decay $B_c^+ \to \tau^+\nu_\tau$ is equivalent to the decay $B_c^- \to \tau^-\bar{\nu_\tau}$. Furthemore, the lepton number must be conserved. The three different lepton numbers are the electron lepton number, muon lepton number and tau lepton number. This conservation of lepton number can be observed in Feynman diagrams since for each of the leptonic vertices, there is one arrow pointing into the vertex (so anti-lepton, so $L = -1$) and one pointing out of it (so lepton, so $L = 1$) and both lines concern the same lepton. The B_c meson, the subject of this thesis, can decay through weak annihilation using a virtual W boson [12]. This B_c meson contains two flavor-asymmetric quarks, bottom and charm, which cannot annihilate to a gluon or photon [13]. This eliminates the strong and electromagnetic interactions, which makes the B_c meson a good meson to study weak decays of heavy quarks. The purely weak annihilation can be visualized in Feynman diagram 2.

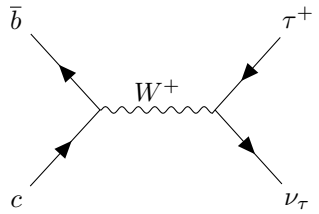

Figure 2: Purely weak annihilation of B_c^+ meson.

The B_c meson can furthermore decay according to the simple spectator quark model. This is possible via a bottom quark decay with a charm spectator quark, see figure 3, and a charm quark decay with an anti-bottom spectator quark, see figure 4. [13]

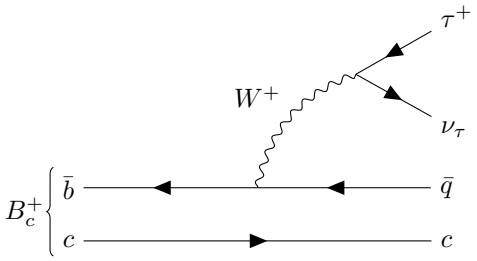

Figure 3: Bottom quark decay with charm spectator quark, with 'q' being either a charm or an up quark.

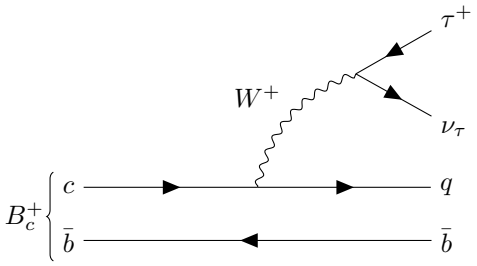

Figure 4: Charm quark decay with charm spectator quark, with 'q' being either a strange or a down quark.

The decay modes shown in figure 3 and 4 are semileptonic decays, meaning that a hadron decays into another hadron and leptons.

3.4 The CKM matrix

The Cabibbo-Kobayashi-Makawa (CKM) matrix is important to understand the behaviour of quarks and therefore also to understand the decay of the B_c meson. The CKM matrix is an $n \times n$ complex matrix, where n counts the number of generations. Since there are three quark generations, the CKM is a 3x3 matrix.

$$V_{CKM} = \begin{pmatrix} V_{ud} & V_{us} & V_{ub} \\ V_{cd} & V_{cs} & V_{cb} \\ V_{td} & V_{ts} & V_{tb} \end{pmatrix}$$

The CKM matrix is non-diagonal, with the off-diagonal terms implying that weak-interaction transitions between quark generations are allowed, which is called quark mixing. Therefore, the CKM matrix governs all flavor changing transitions between different types of quarks (up-type quarks to all down-type quarks and down-type quarks to all up-type quarks) in the SM. The elements V_{ij} connect the ith left-handed up-type quark to the jth left-handed down-type quark. [14]
Quark mixing is however always suppressed compared to the quark transitions within a generation. This suppression can also be noticed from the sizes of the CKM elements of the non-diagonal and diagonal elements in the following matrix [15]. [16, 17]

$$V_{CKM} = \begin{pmatrix} 0.974353 & 0.22500 & 0.003667 \\ 0.22487 & 0.973521 & 0.04145 \\ 0.008519 & 0.04065 & 0.999142 \end{pmatrix}$$

The values in this matrix are obtained by the CKMfitter group which determines the CKM matrix elements, like V_{cb}, using a global fit.

CKMfitter The CKM matrix defines four parameters for the weak charged current interactions of quarks. These four parameters can be determined using different parametrizations. A commonly used parametrization is the Wolfenstein parametrization. This parametrization allows the CKM matrix to be expressed in terms of $\lambda, A, \bar{\rho}, \bar{\eta}$. The lambda parameter is approximately equal to 0.22. The other

matrix elements are rewritten in terms of these four parameters as an expansion of λ [18], which results in the following matrix. [19]

$$V_{CKM} = \begin{pmatrix} 1 - \frac{\lambda^2}{2} & \lambda & A\lambda^3(\rho - i\eta) \\ -\lambda & 1 - \frac{\lambda^2}{2} & A\lambda^2 \\ A\lambda^3(1 - \rho - i\eta) & -A\lambda^2 & 1 \end{pmatrix}$$

The unitarity of the CKM matrix implies certain relations between its elements, some of which can be visualized in the complex plane as a so-called unitarity triangle (UT). The best example of this is the orthogonality condition between the third and first column of the CKM, namely $V_{ud}{V_{ub}}^* + V_{cd}{V_{cb}}^* + V_{td}{V_{tb}}^* = 0$ [18]. After rescaling the triangle by dividing all sides by $V_{cd}{V_{cb}}^*$, the triangle gets the coordinates (0,0), (1,0) and $(\bar{\rho}, \bar{\nu})$ and can be displayed as figure 5.

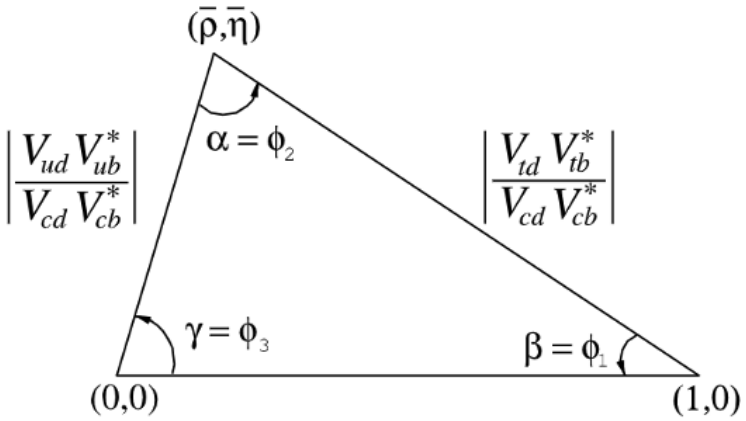

Figure 5: Unitarity triangle using parameters of Wolfenstein parametrization. [17]

The CKMfitter group determines the CKM matrix elements using a global fit to all available measurements of UT parameters. The most recent global fit is from the 2021 CKMfitter group, which can be visualized in figure 6.

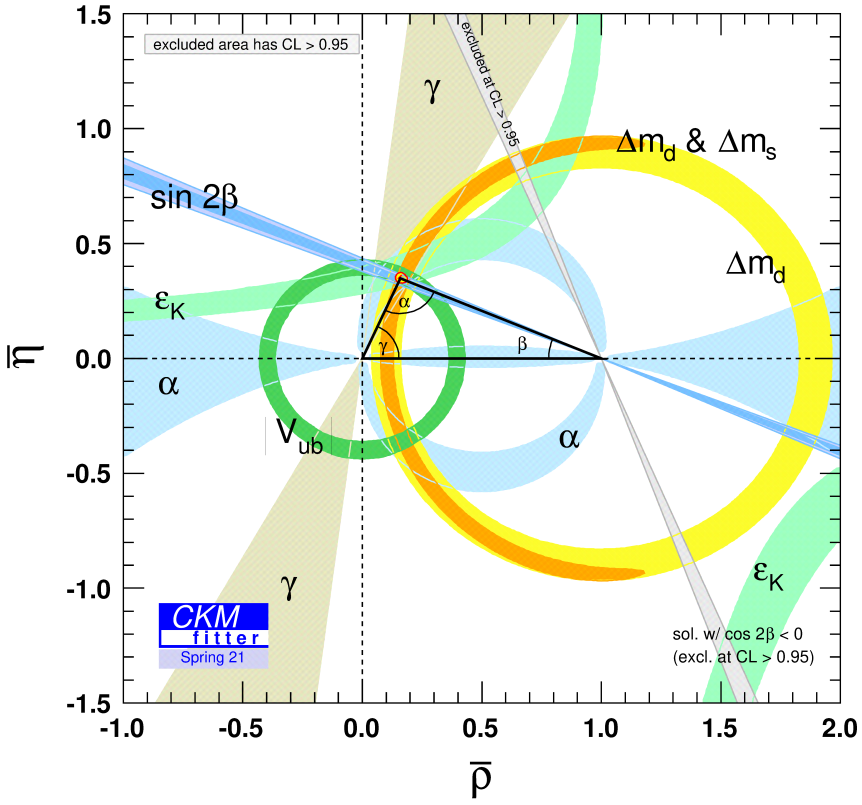

Figure 6: The global CKM fit in the large $\bar{\rho}, \bar{\eta}$ plane. The constraints on the UT parameters can be observed as the colored fields in the figure. [15, 18]

V_{cb} The V_{cb} parameter is one of the elements of the CKM matrix for $b \to c$ quark transitions. The 2021 updated V_{cb} value from the CKMfitter group [15] is determined to be value (1).

$$|V_{cb}| = (41.45^{+0.35}_{-0.61}) \times 10^{-3} \tag{1}$$

This V_{cb} value is thus an average including numerous experimental measurements. It will not be used for an updated prediction of the branching fraction, since the value is merely an average which covers up the information of individual measurements of either exclusive or inclusive determinations. It is therefore only mentioned as a reference value for the current world average of V_{cb}.

To determine the value of the V_{cb} CKM matrix element directly, experimental measurements from exclusive and inclusive reconstruction of semileptonic decays of B mesons can be used. Exclusive reconstructions use single hadronic channels, while inclusive reconstructions use a sum of all hadronic channels. The exclusively and inclusively determined values give conflicting results, which is a long-standing discrepancy in V_{cb} determinations. This difference between exclusive and inclusive determinations is therefore an important problem to consider for computing the value of the branching fraction of $B_c^+ \to \tau^+ \nu_\tau$.

3.5 Exclusive determinations

For exclusive determinations, CKM elements, like V_{cb}, can only be extracted using both the external experimental decay observables and the form factor of the specific decay mode. To understand the V_{cb} determination from these quantities, some more context about recoil is needed. Therefore, recoil will be explained first, followed by a short discussion of both the decay quantities and the form factor, ending with a discussion on how to combine them.

Recoil Zero-recoil is when the recoil parameter, ω, is equal to 1 (normalized). This recoil parameter can be expressed as $\omega = \nu \times \nu'$, which is the product of the four-velocities of the decaying meson and the formed meson, for example the $\bar{B}$ and D^* meson four-velocities for the $\bar{B}^0 \to D^{*+}\ell^-\bar{\nu}_\ell$ decay. In this example, the zero-recoil point corresponds to the kinematical situation were the D^* meson stays at rest in the rest frame of the decaying $\bar{B}$ meson. This means that a higher energy was transferred to the formed leptonic pair. Therefore, at the zero-recoil point, the momentum transferred to the leptonic pair, q, is maximum. So, a low value of ω corresponds to the high q^2 region. [20]

Experimental decay measurements As ω goes to 1, so to zero-recoil, the differential decay width, expressed in ω as for example in Eq. (2), vanishes [21]. This can be observed in Eq. (2) since the term $\omega^2 - 1$ becomes 0 when $\omega = 1$. Therefore, the experimental decay measurements are mostly performed at higher recoil, so in the lower q^2 region.

$$\frac{d\Gamma}{d\omega}(\bar{B}^0 \to D^{*+}\ell^-\bar{\nu}_\ell) = (1+\pi\alpha)\frac{{G_F}^2 {M_{D^*}}^3}{4\pi^3}(M_B - M_{D^*})^2(\omega^2-1)^{1/2}X(w)|V_{cb}|^2|\eta_{EW}F(\omega)|^2 \quad (2)$$

where $X(w)$ is the phase space factor, η_{EW} accounts for the leading electroweak corrections, $(1+\pi\alpha)$ accounts for the Coulomb attraction of the final-state charged particles and $F(\omega)$ is the form factor from QCD [21]. A graphical representation of this relation between the decay width and the recoil parameter can be observed in figure 7. [22, 23]

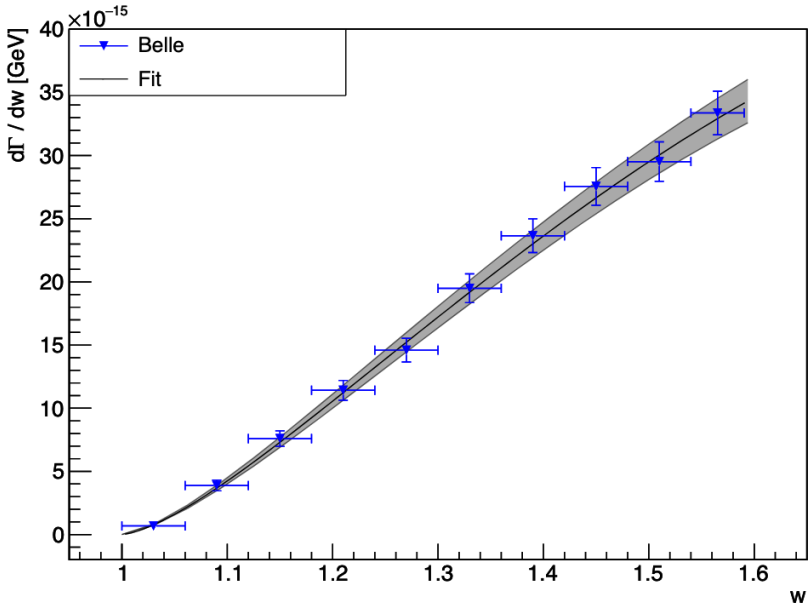

Figure 7: Fit to the measured $\Delta\Gamma/\Delta w$ spectrum of the decay $B \to Dl\nu_l$, performing extrapolation to $\omega = 1$ using the CLN parameterization. The respective uncertainty of each data-point is shown by vertical error bars and the bin widths by horizontal bars. The solid curve corresponds to the result of the fit and the surrounding grey area indicates the uncertainty in the coefficients of the CLN parameters. [24].

Lattice form factor The second component needed to calculate V_{cb} in exclusive determinations are form factors. These form factors can be obtained from lattice QCD, which will be more elaborately discussed in section 4. These lattice calculations are most accurate at high q^2, so in the low recoil region. Most form factor calculations are therefore performed at zero-recoil, so $\omega = 1$. These form factors can be used for normalization.

Combination of both quantities to obtain V_{cb} As said before, V_{cb}, can only be extracted using both the experimental decay measurements and the form factor information. Since the experimental measurements are most accurate at low q^2, while the lattice form factors are most accurate at high q^2, it is necessary to extrapolate the quantities found from the decay to the zero-recoil point in order to combine both.

The differential decay rate of a certain decay mode can be given in terms of a function $F(w)$, which is the form factor over the whole recoil region. Therefore, to perform an extrapolation to the zero-recoil point, the function $F(\omega)$ has to be expressed in terms of parameters. Different parameterizations have been suggested to describe this $F(\omega)$.
In the past, most research groups used the CLN parameterization. However, in 2017, a new unfolded data set released by the Belle collaboration [25] triggered several theoretical analyses [23, 26, 27] to compare the effect of the choice of a specific parameterization on the V_{cb} value. It was found that the CLN parameterization did not describe the experimental data good enough, whereas the BGL parameterization did and the resulting V_{cb} exclusive value was also compatible with the inclusive V_{cb}. This was however contradicted again by computations of the Belle Collaboration using their own full data set [28] and other more recent publications. The Belle Collaboration made a direct comparison between the parameterizations to discover that the BGL parametrization gives a value for V_{cb} that is consistent with the CLN parametrization. Therefore, the contradiction between exclusive and inclusive V_{cb} determinations remains and there is still no consensus about the use of parameterization.

3.6 Hints for BSM physics

The SM includes the electroweak theory and quantum chromodynamics (QCD). As the name implies, the electroweak theory includes the electromagnetic force and the weak nuclear force. QCD is the theory that describes the strong nuclear force in the SM. Therefore, the SM describes three of the four fundamental forces. This also directly indicates a problem of the SM, namely the exclusion of the gravitational force. Another problem is the lack of explanation by the SM for the matter-antimatter asymmetry that we observe in our universe.
Other hints of violation of the SM can be found when comparing branching fractions of decays that only differ in their lepton flavor. The experimentally determined ratio between the branching fractions can be compared with the prediction of this ratio by the Standard Model. An example of this is the ratio of the branching fractions $B \to D^{(*)}\tau\nu_\tau$ over $B \to D^{(*)}\ell\nu_\ell$ with ℓ being e or μ. This ratio is called $R(D^{(*)})$. From comparing these ratios to the SM prediction, a discrepancy between the experimental measurements and theoretical expectation value was found. These measurements were performed by Belle, BaBar and LHCb [29–36]
An overview of all these $R(D)$ and $R(D^*)$ measurements is produced by the Heavy Flavor Lattice Averaging Group (HFLAV) [5]. A recent update of this overview, which can be observed in figure 8 also includes a new joint measurement of $R(D)$ and $R(D^*)$ by LHCb. In this figure, the experimental results for combined $R(D)$ and $R(D^*)$ measurements are shown as ellipses and the individual measurements of $R(D^*)$ are shown as bands (from single points with error bars). The updated HFLAV average, which can be observed as the red ellipse, exceeds the SM prediction by 3.2σ. This means that the average is still in agreement with the SM since these 3 standard deviations are not enough deviation to call the values inconsistent. In particle physics, the values are determined to differ enough to call the result a new discovery when they differ by 5σ, so 5 standard deviations. These kinds of violations of the Standard Model can be evidence for BSM.

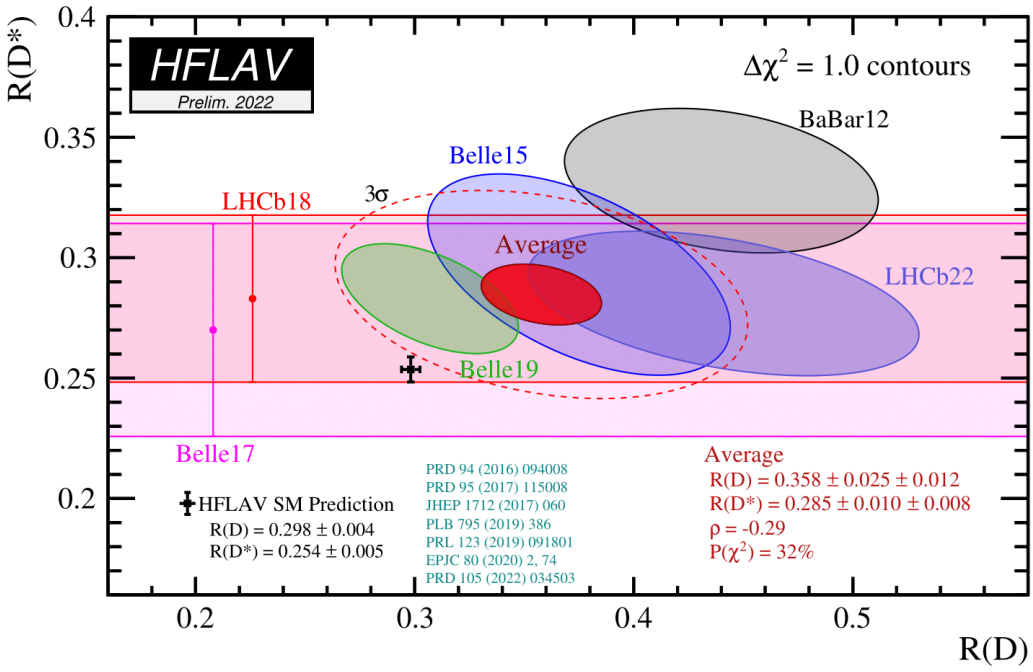

Figure 8: Measurements of the ratios $R(D)$ and $R(D^*)$ combined into a two-dimensional figure. The contours correspond to $\Delta\chi^2 = 1$, so the edges of the error contours are exactly one standard deviation. The newly obtained LHCb result is shown as a purple ellipse and the new preliminary HFLAV average of the $R(D^*), R(D)$ ratios is shown as the red ellipse in the middle. The dashed red ellipse corresponds to a 3σ deviation from the computed HFLAV average. The prediction of the SM can be observed as the black dot with its respective error bars. [5]

4 Lattice QCD

QCD is the theory that describes the strong nuclear interaction in the SM. QCD describes interactions that are mediated by massless spin-1 bosons, called gluons. Theories of this type are called gauge theories since they are based on a symmetry called gauge invariance. The gluons are its gauge bosons.
At short distances, thus at a high energy scale (high q^2), QCD has a property called asymptotic freedom. Asymptotic freedom implies that the interaction strength, α_s, reduces at short distances. This reduction of interaction strength between quarks allows for perturbative calculations.
On the contrary, as the distance between the quarks increases, thus at a lower energy scale (low q^2), the quark interaction gets stronger. This property of QCD at larger distances is called quark confinement. Increasing interaction strength allows for many higher order interactions, which makes the calculation very complicated. Therefore, at the low-energy part of QCD (long-distance physics), calculations can only be performed using numerical simulations of the QCD theory on a space-time lattice on a computer. These calculations are called non-perturbative calculations. [11, 37]

Lattice QCD The non-perturbative method used for solving QCD theory is called lattice QCD (LQCD). In LQCD, the lattice is made up of a discrete set of space-time points. The lattice is usually constructed as a 4D hyper-cube with lattice-spacing a. Its four-dimensions include three spacial dimensions and one temporal dimension. This simplification of space-time allows for numerical QCD computations when the quarks are placed on the sites of the hyper-cubic lattice and the QCD gauge field is placed on the links between these sites [38, 39].
These LQCD calculations can in principle calculate QCD quantities to arbitrary accuracy on a computer. However, the LQCD calculations are in practice limited by the computational resources and efficiency of algorithms since the calculations require ever more computing power to deliver more accurate calculations.
LQCD results are accompanied by both a statistical and a systematic error. The statistical error comes from the Monte-Carlo integration. The Monte-Carlo method is used to calculate the Feynman Path Integral numerically [40]. This numerical integration needed for LQCD calculations uses randomly chosen points at which the integral is evaluated, so the outcome approximates the correct value with respective error bars. The systematic error comes from inaccuracies inherent to the system for example the use of non-zero values of the lattice spacing a. This is because zero lattice spacing cannot be reached, since the computational cost grows with a decreasing a. [39]

Simulating fermions on the lattice To be able to simulate fermions on the lattice to perform LQCD calculations, the so-called fermion action needs to be discretized. This discretization is needed since the lattice is also made up of a discrete set of space-time points instead of being continuous. The simplest discretization is the so-called naive fermion action. A problem of this naive fermion action is that it suffers from the fermion doubling problem.
This problem arises due to formulating naive lattice fermions to have chiral symmetry. It is important to maintain the chiral symmetry of fermions in the LQCD simulations since this is one of the properties of a fermion that is needed to allow it to interact in the strong interaction [41]. This maintaining of chiral symmetry can only be realized when, for d dimensions, lattice QCD produces 2^d equivalent fermion fields in the continuum limit. Since the lattice used in LQCD is a four-dimensional grid, LQCD simulates sixteen equivalent fermion fields in the continuum limit. This introduction of unwanted doubler fermions is called the fermion doubling problem. [39]

LQCD for the B_c meson decay On top of this fermion doubling problem, another problem arises specifically for the B_c meson decay. This problem has to do with the need to simulate quarks on the lattice. Simulating quarks onto the lattice works well when $am_q << 1$, where a is the lattice spacing and m_q is the quark mass. So, LQCD works well when the quark mass is small compared to the lattice cut-off. However, when this condition is not met, lattice QCD simulations give large errors. These large errors arise because some of the discretization errors are proportional to powers of am_q, so become large when am_q is bigger than 1. Lattice QCD simulations are therefore not helpful in analyzing heavy quarks, since the errors are too large when the mass is high. This problem arises when looking at the B_c meson, since it contains an intermediately heavy charm quark and a heavy bottom quark. The currently available lattice spacing causes $am_b \not< 1$, whilst the charm quark is an intermediate case. [39,42]

4.1 Highly Improved Staggered Quark action

The fermion doubling problem can be tackled by using staggered fermion action instead of naive fermion action to discretize fermions onto the lattice. This staggered fermion action, like naive fermion action, retains the chiral symmetry of the fermions. Staggered fermions are a reduced version of naive fermions with the difference being the partial removal of their Dirac structure. Only a single fermion Dirac component remains on each lattice site. The staggered fermion formulation can reduce the number of doublers to three, so staggered fermion formulation produces four fermion flavors per one continuum flavor. These four degenerate fermion flavors, nonphysical species of quarks, are known as tastes. By taking the fourth-root of the fermion determinant in its path integral, the three unwanted tastes can be removed. Using staggered fermion action however causes new problems like taste-symmetry breaking that can cause large discretization errors. [22, 39]
These problems can in turn be solved by using highly-improved staggered quark action (HISQ), first introduced by ref. [43]. HISQ adds additional terms to the lattice action which suppresses taste-symmetry breaking and reduces some of the discretization errors, including $O(a^2)$ and $O(am_q)^n$. Therefore, the fermion doubling problem is solved using HISQ.
The remaining problem to simulate the heavy quarks of the B_c meson onto the lattice is also be addressed by HISQ. As said before, the problem with simulating this B_c meson onto the lattice are the discretization errors proportional to powers of am_q. Since HISQ suppresses these $O(am_q)^n$ errors, this method is also useful for the B_c meson containing heavier quarks where the error would otherwise become too high. Charm quarks can be directly simulated using HISQ and using very fine lattice spacings enables simulations of the bottom quark mass close to the physical bottom quark mass [43, 44]. To also use the HISQ formulation for these bottom quarks, extrapolation in m_b is needed. This extrapolation makes use of the mass dependence predicted by the heavy quark effective theory (HQET). This HQET uses heavy quark symmetry to make accurate predictions about heavy quarks whilst controlling the theoretical errors. The extrapolation in the heavy-quark mass up to the physical bottom quark mass and the extrapolation to zero lattice spacing (both extrapolations to continuum) that are needed using HQET are important sources of error that remain for HISQ calculations [45]. Another important source of error for HISQ calculations are statistical errors from the extrapolation fit and errors from the shifts to include missing real world effects like electromagnetism.

Heavy Quark Effective Theory HQET is an effective field theory which can be used for non-perturbative QCD calculations like LQCD by providing an extrapolation of heavy quark masses. This extrapolation then allows the use of the HISQ formulation in LQCD for bottom quarks on the lattice, thus for B_c^+ meson calculations.
HQET works by performing a systematic expansion in the powers of Λ_{QCD}/m_q, with well-defined errors. In this expansion, HQET uses the heavy quark limit $m_q \to \infty$. This approximation enables non-perturbative treatment of heavy quarks. To obtain quantitative results from these calculations using the heavy quark limit, some corrections have to be included since the quark masses are not infinite [46]. Firstly, power corrections in the expansion in Λ_{QCD}/m_q need to be included. These power corrections are most needed for Λ_{QCD}/m_c, since this term is bigger than Λ_{QCD}/m_b as m_c is smaller than m_b. Furthermore, logarithmic corrections need to be included since some quantities depend on the strong coupling constant which depends on m_q logarithmically. HQET incorporates these and other corrections, for example also radiative corrections, in its theory to perform calculations.
Therefore, it is possible to make calculations with well-defined errors by performing a systematic expansion in the powers of $\Lambda_{QCD}/m_{b,c}$. This means that HISQ combined with HQET solves both the fermion doubling problem and the heavy quark mass problem. HISQ combined with HQET can therefore be used to simulate charm and bottom quarks and therefore the B_c^+ meson onto the lattice for LQCD calculations [38, 44].

4.2 Nonrelativistic QCD

An entirely different solution to the LQCD problems, other than the HISQ formulation using HQET, is discretizing the bottom quark using improved non-relativistic QCD (NRQCD). NRQCD is in principle used for heavy-heavy, quarkonium, systems which are a bound state of a heavy quark and its respective heavy anti-quark. However, it can also be used for other systems, like the flavored B_c meson. It can be used for the bottom quark of the B_c since the typical velocity of a bottom quark inside a hadron is non-relativistic [47, 48]. This approach would be less successful for charm quarks, since their smaller

mass makes them much less non-relativistic [43].
A big advantage of NRQCD is that the discretization errors are much easier to control since no extrapolation in m_b is needed. On the other hand, the NRQCD operators have a non-relativistic expansion and must have their normalization matched to the normalization of the appropriate continuum operator. Both the non-relativistic expansion and the normalization problem introduce systematic uncertainty into its results [49]. Another disadvantage of NRQCD is that some of the parameters need to be determined perturbatively. Perturbative calculations describe a complicated quantum system in terms of a simpler one (for which the mathematical solution is known) and work by adding an additional perturbing Hamiltonian representing a weak disturbance to the system. The physical quantities of the slightly perturbed system can then be expressed as corrections to the quantities of the simple system. These corrections are small compared to the size of the quantities themselves, which means that these values can be used for approximate calculations. So, including perturbative calculations limit the precision of the final results [39, 48].

5 The branching fraction

A branching fraction is the probability of the decay via a specific decay mode. It indicates the fraction of particles that decay via this mode as part of all possible decay modes, with a total of 1. Therefore, a branching fraction has a numerical value between 0 and 1.

5.1 The branching fraction formula

The numerical SM prediction for the branching fraction of the $B_c^+ \to \tau^+\nu_\tau$ decay can be determined using the following formula [6, 7]:

$$\mathcal{B}(B_c^+ \to \tau^+\nu_\tau)^{SM} = \frac{G_F^2}{8\pi} |V_{cb}|^2 f_{B_c}^2 \tau_{Bc} m_{Bc} m_\tau^2 \left(1 - \frac{m_\tau^2}{m_{Bc}^2}\right)^2 \tag{3}$$

In formula (3), G_F is the Fermi coupling constant, $|V_{cb}|$ is a matrix element of the Cabibbo-Kobayashi-Maskawa (CKM) matrix for the transition between the c and b quarks of the B_c meson, f_{B_c} is the B_c meson decay constant, m_{Bc} is the B_c meson mass, m_τ is the tau lepton mass and τ_{B_c} is the meson lifetime.

The units of all parameters in this thesis are given according to the natural units system, which sets $\hbar$ (reduced Planck constant) and c (speed of light) equal to one. This means they can be omitted from the unit of a parameter. For example the Fermi coupling constant, denoted by G_F using the natural unit system, is in fact described by $\frac{G_F}{(\hbar c)^3}$.

The numerical value of the branching fraction can be determined when the values of all parameters in the formula are known. Ref. [6] performed this computation and predicted the following numerical value for the branching fraction $B_c^+ \to \tau^+\nu_\tau$:

$$\mathcal{B}(B_c^+ \to \tau^+\nu_\tau)^{SM} = (1.95 \pm 0.09) \times 10^{-2} \tag{4}$$

Ref. [7] also performed this computation and determined the following numerical value:

$$\mathcal{B}(B_c^+ \to \tau^+\nu_\tau)^{SM} = (2.25 \pm 0.21) \times 10^{-2} \tag{5}$$

I have tried to reproduce both the value (4) computed by ref. [6] and the value (5) computed by ref. [7] as a check for further calculations of the inclusive and updated branching fractions. The value of (4) could be almost exactly reproduced as (6) using their input values, with a small difference visible which could be due to different rounding or slightly different input values (since not all input values were available). This was however not the case for the value (5) as its numerical branching fraction could not be reproduced using the exact same input values that were used in the article (see table 19 of ref. [7] for an overview of their input values). The numerical value that was calculated instead is (7).

$$\mathcal{B}(B_c^+ \to \tau^+\nu_\tau)^{SM} = (1.96 \pm 0.10) \times 10^{-2} \tag{6}$$

$$\mathcal{B}(B_c^+ \to \tau^+\nu_\tau)^{SM} = (2.07 \pm 0.20) \times 10^{-2} \tag{7}$$

The reproduced values (6) and (7) will be used as the exclusive predictions to be analyzed for the remainder of this thesis.

Ref. [7] furthermore mentions an inclusively determined value for V_{cb}:

$$|V_{cb}| = (41.62^{+0.26}_{-0.80}) \times 10^{-3} \tag{8}$$

Using this inclusively determined V_{cb} value, the numerical prediction of the branching fraction of the decay $B_c^+ \to \tau^+\nu_\tau$ is found to be (9).

$$\mathcal{B}(B_c^+ \to \tau^+\nu_\tau)^{SM} = (2.29 \pm 0.19) \times 10^{-2} \tag{9}$$

The exclusively determined value, (7), has an uncertainty that is more than twice as high as the uncertainty accompanying exclusive prediction (6). Furthermore, inclusive prediction (9) has a numerical value that is higher than the exclusive predictions. These differences can be investigated by looking into the parameters of the formula.

5.2 Parameter error analysis

In this section, firstly the theory behind errors and error propagation is discussed, followed by an error analysis of the parameters used for computing the branching fraction value.

5.2.1 Error theory

All measurements come with a certain degree of uncertainty. These uncertainties arise since quantities cannot be measured exactly. As measurement results are often used to calculate some other quantity, an error in the measurement will also lead to an error in the final calculated quantity. To describe how errors propagate and influence the final result, error analysis is used. [50]

There are two different kinds of errors, so-called random (statistical) errors and systematic errors. Random errors are caused by random fluctuations in the experiment, which means that their sign and magnitude vary statistically when the measurement is repeated. On the other hand, systematic errors have the same sign and magnitude upon repeated measurement, which means they will not reveal upon repeated measurement.

Random (statistical) errors could be due to slight fluctuations in the environment, measurement instrument or the way that the value is read from a scale [51].
If a large number of repeated measurements is performed of a single quantity, these errors can be derived from the statistical spread in the results. The error is usually defined such that 68% of the measurement results does not differ more than the error from the true value, which is one standard deviation. If however only a single or a few measurements are performed, an estimate has to be made of the uncertainty in the result since there are not enough measurements to provide a statistical spread in the results. This estimate should be the error with which it can be reasonably expected that there is a probability of 68% that the difference between the measured and the true value is not greater than the assigned error. [52]

Systematic errors are often methodical (measurement instrument influences the quantity to be measured) and instrumentation errors (due to the calibration accuracy of an apparatus) [51].
These systematic inaccuracies are reproducible, but difficult to detect since they will not reveal upon repeated measurement as they cannot be distinguished from the measurement value. Systematic errors can therefore not be eliminated by adding more measurements. This error can only be corrected for if its sign and magnitude are known from other unrelated and independent measurements. Using these results, the systematic error can be (partially) eliminated from the final result by an appropriate correction. In practice, unrelated and independent measurements are often not available, which means the systematic error cannot be corrected for and is propagated into the final result.

5.2.2 Error propagation

To analyze how errors of separate parameters influence the final result, the propagation of errors has to be calculated. For each parameter, its contribution to the error of the final result can be calculated separately and then the squares of the individual errors are added to give the square of the resulting error, which is called the quadratic addition of errors. For example, for the equation $Z = A^n B$, an error is obtained according to Eq. (10). Several of these standard error relations have been derived, which can be used to calculate the error of the branching fraction. [52, 53]

$$\Delta Z = Z\sqrt{(n \times (\frac{\Delta A}{A})^2 + (\frac{\Delta B}{B})^2} \tag{10}$$

5.2.3 Error analysis

In order to have a better look at the errors of all the branching fraction parameters, the errors can be graphically displayed by dividing the errors by their respective value, resulting in figure 9.

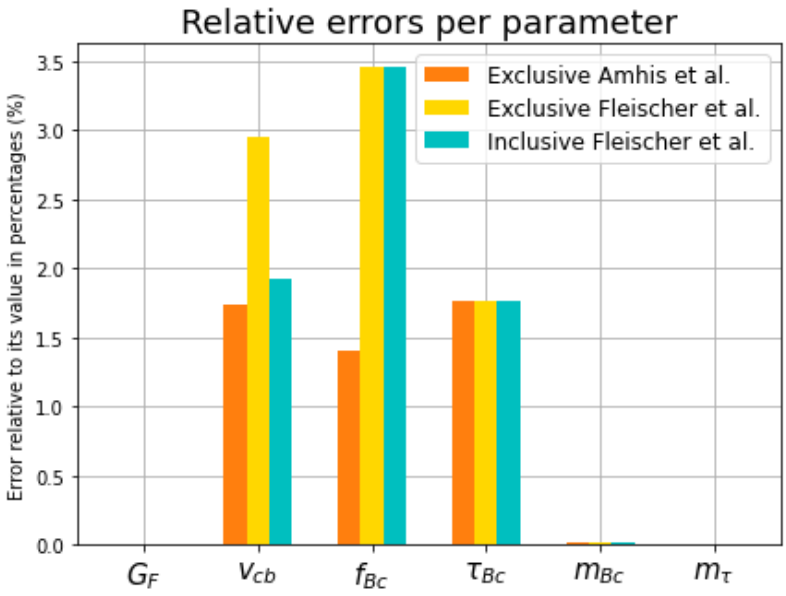

Figure 9: Errors of all parameters of the branching fraction formula, relative to their values.

What stands out most from figure 9 is that the relative errors of G_f, m_{Bc} and m_τ are much lower than the relative errors of the other parameters. These parameters have small uncertainties. Furthermore, some significant differences can be observed between the error fractions of the parameters used by ref. [6] and ref. [7].
To further investigate the error fractions, it is important to look at how the parameter errors propagate into the branching fraction error. To visualize this, a figure can be made of the error contribution of the different parameter errors to the total branching fraction error. These error contributions are calculated using eq. 10. An overview of the results can be visualized as a bar plot in figure 10. The results can also be separated per numerical prediction into individual pie plots in figure 11 to clearly show the contribution of each parameter to the branching fraction error.

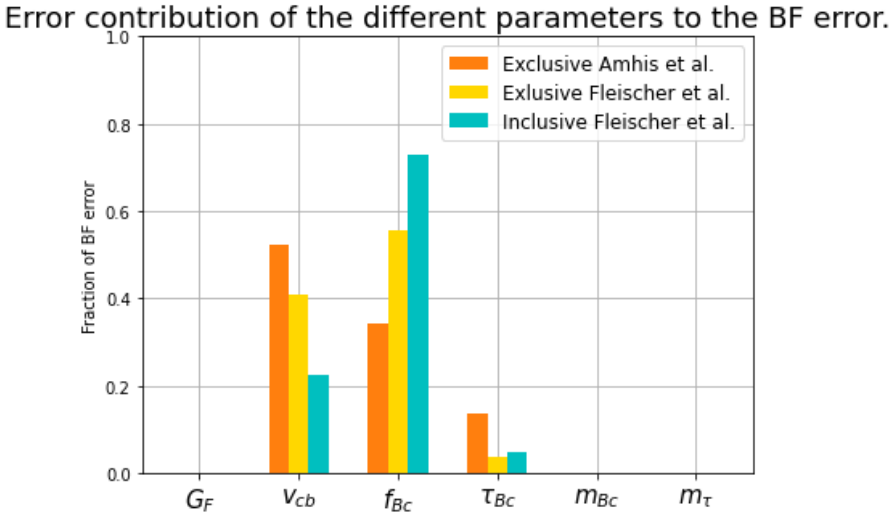

Figure 10: Error contribution of the error of each parameter is expressed as a fraction of the total branching fraction error.

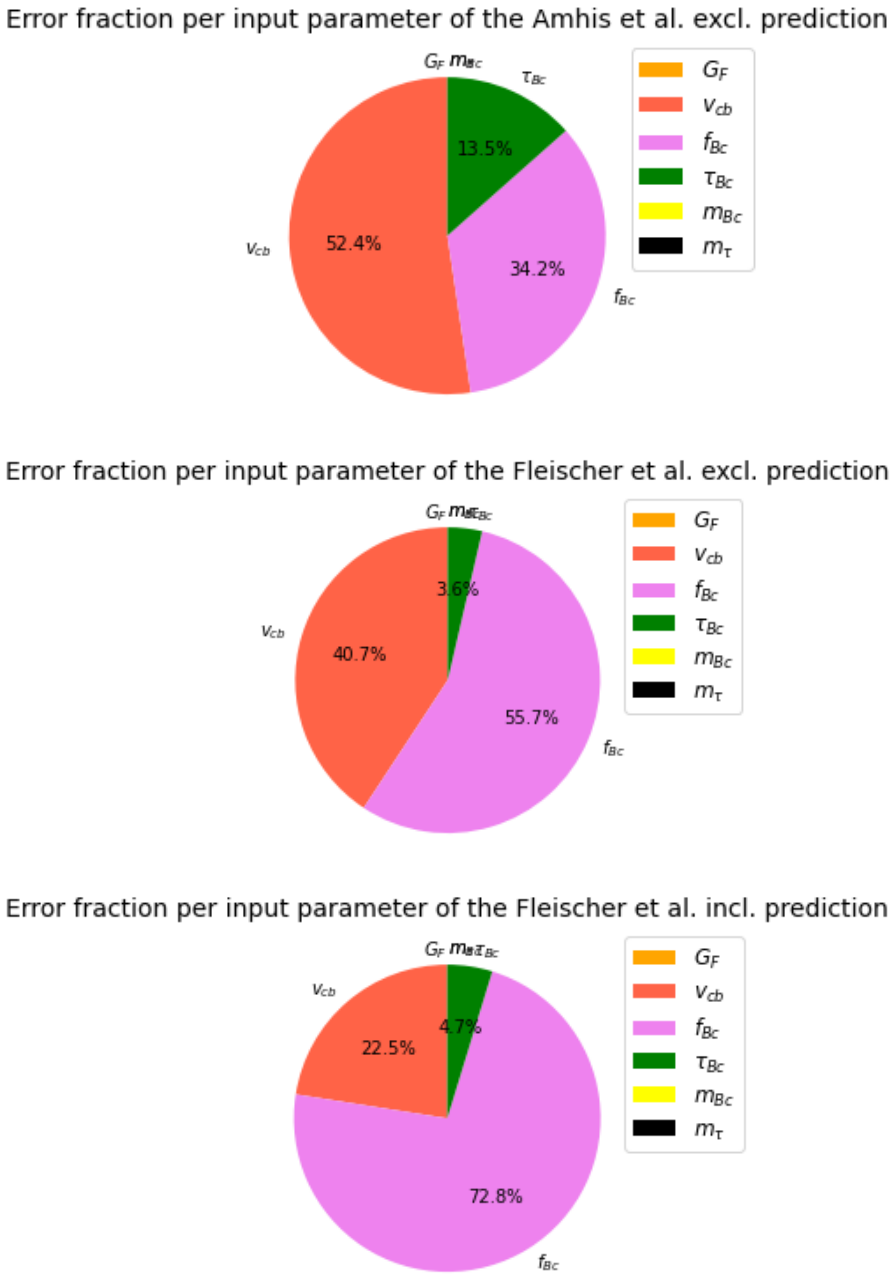

Figure 11: Error contribution of the error of each parameter is expressed as a percentage of the total branching fraction error for all predictions separately.

From figure 10, it can be concluded that the errors of the V_{cb} and f_{B_c} parameters have the biggest error contribution to the branching fraction error. In this figure, there are also clear differences visible between the parameter error contributions of the different predictions. This can be observed even more clearly from the pie plots in figure 11. From these pie plots, it becomes clear that for the ref. [6] prediction, the biggest contribution to the branching fraction error comes from the V_{cb} error. On the other hand, the biggest contribution to the branching fraction error for the ref. [7] prediction comes from the f_{B_c} error. This difference in contribution per parameter in the ref. [7] prediction is even more pronounced for the inclusive prediction, since the error of the inclusively determined V_{cb} value is twice as low as the error for the exclusively determined V_{cb} value. Therefore, the V_{cb} error contribution to the total branching fraction error is lower for the ref. [7] inclusive prediction. This makes V_{cb} and f_{B_c} important parameters to consider for investigating the differences between the branching fraction values. Therefore, the focus of this thesis will lie on these parameters. The f_{B_c} and V_{cb} parameters will be

closely examined in section 6 and section 7, respectively. The other parameters are shortly discussed in the sections 5.2.3.1 and 5.2.3.2 below.

5.2.3.1 The Fermi coupling constant, τ lepton mass and B_c meson mass The Fermi coupling constant is determined experimentally and specifies the coupling by a W boson in weak interactions. This coupling can be approximated as a four-point interaction, since the range that the W boson travels is short.
The value of this Fermi coupling constant, the mass of the B_c meson and the mass of the tau lepton can be obtained from the Particle Data Group (PDG) [39]. The input parameters of the analyzed predictions were all obtained from the 2018 PDG, but two of them, G_F and m_{B_c} were slightly updated in the 2022 PDG review [17, 54]. The tau lepton mass value however remains the same in the 2022 PDG compared to the 2018 PDG and can be found in (11).

$$m_\tau = (1776.86 \pm 0.12) \times 10^{-3}\ GeV/c^2 \tag{11}$$

The input parameters and slightly updated parameters can be summarized in the following tables:

G_F	Value	Error	Unit	Reference
2018	1.1663787×10^{-5}	0.0000006×10^{-5}	GeV	[39]
Updated, 2022	1.1663788×10^{-5}	0.0000006×10^{-5}	GeV	[17]

m_{Bc}	Value	Error	Unit	Reference
2018	6274.9×10^{-3}	0.8×10^{-3}	GeV	[39]
Updated, 2022	6274.47×10^{-3}	0.32×10^{-3}	GeV	[17]

5.2.3.2 The B_c meson lifetime (τ_{B_c}) τ_{B_c} is the B_c meson lifetime. The HFLAV [55] has found (12) as the 2021 average τ_{B_c} value.

$$\tau_{B_c} = (0.510 \pm 0.009) \times 10^{-12}\ s \tag{12}$$

This average is dominated by two recent measurements from the LHCb experiment.
One 2014 LHCb article, ref. [56], performed τ_{B_c} measurements on the semileptonic decay $B_c^+ \to J/\psi \mu^+ \nu_\mu X$, with $J/\psi \to \mu^+\mu^-$. The B_c meson lifetime was determined to be $(0.509 \pm 0.008_{stat} \pm 0.012_{syst}) \times 10^{-12}$ s.
Another 2015 LHCb article, ref. [57], determined the B_c meson lifetime using an entirely different approach. Using the LHCb data, the difference between the decay width of the hadronic modes $B_c^+ \to J/\psi\pi^+$ and $B^+ \to J/\psi K^+$ was determined. From this difference in decay width and using the expression $\Delta\Gamma \equiv \Gamma_{B_c^+} - \Gamma_{B^+} = \frac{1}{\tau_{B_c^+}} - \frac{1}{\tau_{B^+}}$ and the known B^+ lifetime, the B_c^+ lifetime was obtained. This resulted in a lifetime of $(0.5134 \pm 0.011_{stat} \pm 0.0057_{sys}) \times 10^{-12}$ s in which the systematic error also includes the uncertainty related to the B^+ meson lifetime.
Since both measurements are in good agreement and the uncertainties for both measurements are uncorrelated, a combined value can be computed, where the statistical and systematic uncertainties are added in quadrature, which leads to the value $(0.5114 \pm 0.0093) \times 10^{-12}$ s. A few other measurements, from CMS, CDF and D0, lower the HFLAV average by a fraction to $(0.510 \pm 0.009) \times 10^{-12}$ s, as can be observed in the overview provided by figure 12.

Experiment	Method	Data set		$\tau(B_c^+)$ (ps)	Ref.
CDF1	$J/\psi\,\ell$	92–95	0.11 fb^{-1}	$0.46^{+0.18}_{-0.16} \pm 0.03$	[143]
CDF2	$J/\psi\,e$	02–04	0.36 fb^{-1}	$0.463^{+0.073}_{-0.065} \pm 0.036$	[144]
D0	$J/\psi\,\mu$	02–06	1.3 fb^{-1}	$0.448^{+0.038}_{-0.036} \pm 0.032$	[145]
CDF2	$J/\psi\,\pi$		6.7 fb^{-1}	$0.452 \pm 0.048 \pm 0.027$	[146]
LHCb	$J/\psi\,\mu$	2012	2 fb^{-1}	$0.509 \pm 0.008 \pm 0.012$	[147]
LHCb	$J/\psi\,\pi$	11–12	3 fb^{-1}	$0.5134 \pm 0.0110 \pm 0.0057$	[148]
CMS	$J/\psi\,\pi$	2012	19.7 fb^{-1}	$0.541 \pm 0.026 \pm 0.014$	[111]
Average				0.510 ± 0.009	

Figure 12: Measurements of B_c^+ lifetime [55]

A note regarding the units of the meson decay lifetime; the meson lifetime is measured in seconds, but its unit in the branching fraction formula (3) is in GeV^{-1}. This means that the lifetime has to be converted from s to GeV^{-1} using the following conversion relation: 1 s $= 1.52 \times 10^{24}\ GeV^{-1}$. After converting, the following value for the B_c lifetime is obtained:

$$\tau_{B_c} = (7.75 \pm 0.137) \times 10^{11}\ GeV^{-1} \tag{13}$$

6 The meson decay constant (f_{B_c})

A decay constant is a single number which expresses the amplitude for a meson to annihilate to a single particle, for example to a W boson. The decay constant value has to do with the overlap between the wave-function of the quark and the wave-function of the anti-quark [58]. The decay constant therefore contains information about the meson itself [59]. For the B_c^+ meson, the meson decay constant is described by f_{B_c}. Both ref. [6] and ref. [7] use f_{B_c} values determined by the HPQCD collaboration. This HPQCD collaboration focuses on achieving high-precision results for LQCD calculations, specifically calculations on heavy quarks.

Ref. [6] uses (14), from a 2012 HPQCD article [60], as their f_{B_c} value.

$$f_{B_c} = (0.427 \pm 0.006) \times 10^{-3}\ GeV \tag{14}$$

Ref. [7] uses (15), from a 2015 HPQCD article [59], as their f_{B_c} value.

$$f_{B_c} = (0.434 \pm 0.015) \times 10^{-3}\ GeV \tag{15}$$

An overview of these different values of f_{B_c} can be made using figure 13.

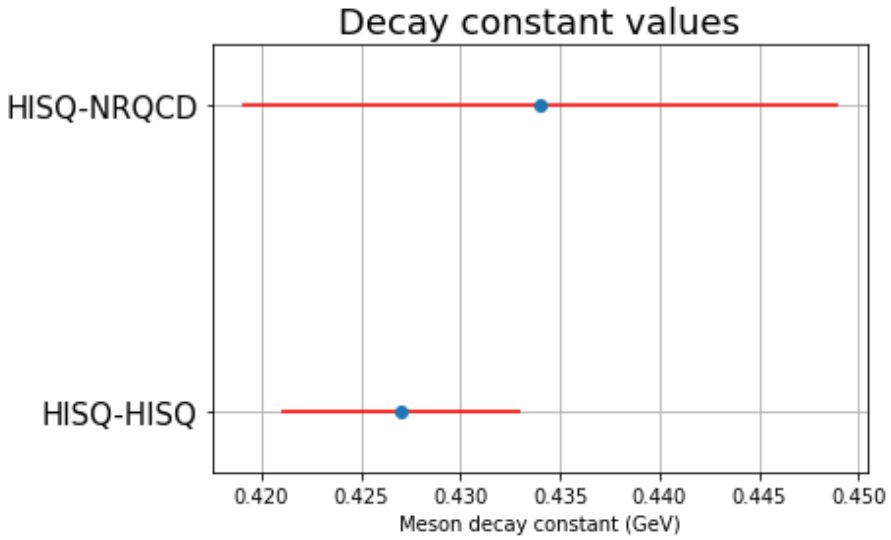

Figure 13: f_{B_c} values and their respective errors. The "HISQ-NRQCD" value is computed by the 2015 HPQCD article [59] used by Fleischer et al. [7] and the "HISQ-HISQ" value is computed by the 2012 HPQCD article [60] used by Amhis et al. [6].

In figure 13, it can be observed that the values agree with each other but differ significantly in their uncertainty. The decay constant determined by ref. [59] using HISQ-NRQCD has an uncertainty that is more than twice the uncertainty of ref. [60] using HISQ-HISQ. Therefore, it is interesting to investigate the differences between the 2012 and the 2015 HPQCD determinations of f_{B_c}.

Both articles use HISQ formulation for the discretization of the charm quark of the B_c^+ meson onto the lattice for LQCD. The articles however differ in their approach to tackle the bottom quark discretization onto the lattice. The 2012 HPQCD article, ref. [60], tackles discretizing the heavy bottom quark onto the lattice by the HISQ formulation, see section 4.1, while the 2015 HPQCD article, ref. [59] tackles discretizing the heavy bottom quark onto the lattice by the NRQCD formulation, see section 4.2.

As said before, the 2012 HISQ-HISQ result has an uncertainty that is twice as small as the 2015 HISQ-NRQCD uncertainty. The HISQ-HISQ result has a lower uncertainty since it uses relativistic formulation which enables the use of simple continuum-like operators that couple to the formed W boson. The advantage of these operators is that they can be chosen to be absolutely normalized [49].

Therefore, no new errors are introduced due to normalization. Furthermore, the error is reduced since the calculation is performed over a wider range of values of the lattice spacing.

6.1 Choice between the HISQ and the NRQCD parameterization

There is no clear reason to prefer either the HISQ-NRQCD or the HISQ-HISQ formulation other than the difference in uncertainty.
Something that should be taken into consideration is the lack of recent f_{B_c} measurements. One recent paper, ref. [61], has investigated the decay constant within the nonrelativistic quark model. This paper produced the following result: $f_{B_c} = 0.439 \pm 0.030 \pm 0.017$ with the first uncertainty due to losing Lorentz covariance and the second uncertainty due to varying the parameter sets. A problem of this result is that it has an even higher uncertainty for the decay constant than the HPQCD results.
Another paper from 2019, ref. [45], has produced updated results for most D- and B-meson decay constants using HISQ-HISQ discretization for LQCD. Ref. [45] was able to calculate the B-meson decay quantities for the first time directly at the physical bottom quark mass. This could be done because of the use of finer lattice spacings than ever before. This reduced the discretization errors to a level small enough to enable the physical bottom quark mass simulation. This direct simulation of the physical bottom quark mass eliminates an important source of uncertainty arising from the otherwise needed extrapolation in the heavy-quark mass up to the bottom quark mass. Their results for B-meson decay constants are about three times more precise than the previous best LQCD calculations performed by HPQCD [60,62]. [45] With this in mind, the 2012 HISQ-HISQ result from ref. [60] is chosen as the current best result as it is anticipated that the HISQ-HISQ formulation is the way to go forward to obtain the most accurate f_{B_c} value.

6.2 Numerical overview f_{B_c}

f_{B_c}	Value	Error	Unit	Discretization	Reference
Amhis et al.	0.427×10^{-3}	0.006×10^{-3}	GeV	HISQ-HISQ	[60]
Fleischer et al.	0.434×10^{-3}	0.015×10^{-3}	GeV	HISQ-NRQCD	[59]
Updated	0.427×10^{-3}	0.006×10^{-3}	GeV	HISQ-HISQ	[60]

7 The V_{cb} parameter

The prediction of the SM decay fraction $B_c^+ \to \tau^+\nu_\tau$ by ref. [6], prediction (6), uses the following exclusive value for V_{cb}:

$$|V_{cb}| = (39.09 \pm 0.68) \times 10^{-3} \tag{16}$$

The prediction of the SM decay fraction $B_c^+ \to \tau^+\nu_\tau$ by ref. [7], prediction (7), uses the following exclusive value for V_{cb}:

$$|V_{cb}| = (39.58 \pm 1.17) \times 10^{-3} \tag{17}$$

An overview of these exclusive V_{cb} values: (16),(17) and the inclusive value (8): $(41.62^{+0.26}_{-0.80}) \times 10^{-3}$, introduced in section 5, can be made using figure 14.

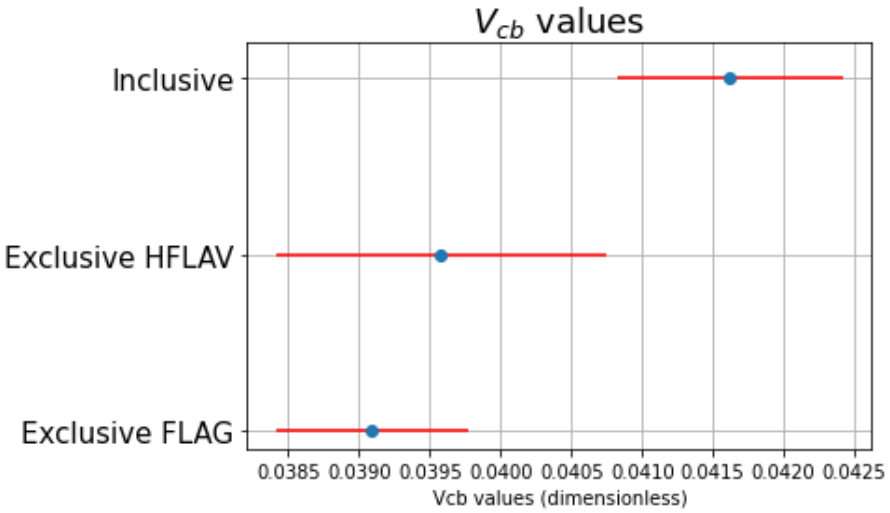

Figure 14: An overview of the "Inclusive" V_{cb} value (8) [7], "Exclusive HFLAV" V_{cb} value (17) [7] and "Exclusive FLAG" V_{cb} value (16) [6] and their respective errors.

In figure 14, it can be observed that the exclusive values are consistent with each other, but are both discrepant with the inclusive value. Since the exclusive and inclusive values do not agree with each other, it is interesting to look at the difference between exclusive and inclusive determinations. Furthermore, there is a clear difference in the size of the uncertainty of the exclusive V_{cb} values, which is another interesting subject for further investigation. Therefore, both determinations will be discussed more elaborately.

Exclusive determinations make use of semileptonic B decays with a specific hadron in the final state. Examples of these exclusive decay modes are to a D or D^* meson, namely $B \to D\ell\nu_\ell$ and $B \to D^*\ell\nu_\ell$. In order to look at such a specific decay and use it for determining V_{cb}, the full hadronic state has to be reconstructed. One also has to take the form factor into account. These form factors need to be calculated non-perturbatively, for which input from lattice QCD calculations is necessary.
An inclusive semileptonic B decay can be described by $B \to X_c\ell\nu_\ell$ in which X_c is the final hadronic state including a charm quark. This means that the inclusive determination uses all B decays involving a $b \to c\ell\nu_\ell$ transition. Therefore, to use an inclusive determination, a theoretical analysis summing all possible hadronic states is needed. This thus means that one sums over all possible final states of the decay, so it is a sum over all possible exclusive decay modes followed by their respective phase space integral (the phase space represents all possible states of a system). Summing over all decay modes simply means that they can be ignored, which is an advantage as this eliminates some hadronic uncertainties.
For calculating inclusive semileptonic decays, operator product expansion (OPE) makes sure that the non-perturbative effects are suppressed by powers of the quark mass and are parameterized by inclusive quantities that can be extracted from experimental data [63]. This OPE works well for heavy quarks, such as the bottom quark, since the non-perturbative effects are suppressed by powers of the heavy quark

mass. This specific form of OPE is called heavy quark expansion (HQE), which is distinct from HQET[1]. For inclusively determining the V_{cb}, the non-perturbative effects are parameterized using parameters that can be measured using observables of $B \to X_c \ell \nu_\ell$ decays, such as the moments of lepton energy and the hadronic invariant mass distributions in semileptonic B decays [55, 63]. The total decay width, which is an inclusive quantity, can be well approximated by HQE as a double-expansion in the strong coupling constant α_s and inverse powers of the heavy-quark mass [64].
To find V_{cb} from inclusive determinations, a global fit is performed. This global fit is a simultaneous fit to the HQE parameters, the quark masses and the absolute values of CKM matrix elements [39, 65, 66]

7.1 Exclusive determination

Exclusive determinations have not only been in conflict with inclusive determinations, but also with themselves. This internal conflict comes from alternative calculations of the hadronic form factors. These alternative calculations arise from different parameterizations, the BGL and the CLN parameterization. Some articles, refs. [23, 26], have shown that these parameterizations lead to different results for the exclusive determination of V_{cb}.

The first prediction of the SM decay fraction $B_c^+ \to \tau^+ \nu_\tau$, prediction (6) by ref. [6], uses the following exclusive value for V_{cb}:

$$|V_{cb}| = (39.09 \pm 0.68) \times 10^{-3} \tag{18}$$

This value was determined by the FLAG 2019 review group [67] using the Boyd, Grinstein, and Lebed (BGL) parametrization for an exclusive determination of the $B \to D^{(*)} \ell \nu_\ell$ decay mode.

The second prediction of the SM decay fraction $B_c^+ \to \tau^+ \nu_\tau$, prediction (7) by ref. [7], uses the following exclusive value for V_{cb}:

$$|V_{cb}| = (39.58 \pm 1.17) \times 10^{-3} \tag{19}$$

This value was determined by HFLAV 2018 review group [55], using the Caprini, Lellouch and Neubert (CLN) parametrization for an exclusive determination of the $\bar{B} \to D \ell^- \bar{\nu_\ell}$ decay mode. This value is in agreement with the value obtained from another hadronic decay mode $\bar{B} \to D^* \ell^- \bar{\nu_\ell}$.
The error is given as one error (added in quadrature) in (19), but can also be separated into an experimental and a theoretical error, as can be observed in (20).

$$|V_{cb}| = (39.58 \pm 0.94_{exp} \pm 0.37_{th}) \times 10^{-3} \tag{20}$$

This separation into an experimental and theoretical error provides some more insight into the origin of the error of the V_{cb} value. The first uncertainty covers for statistical and systematic uncertainties coming from experimental measurements. The second uncertainty covers the theoretical uncertainty coming from LQCD calculations and electroweak corrections. The electroweak corrections come from the radiative corrections of the HQET calculations.

7.1.1 Form factors from LQCD

Next to this difference in used parameterization, the exclusive V_{cb} predictions also differ in the used form factor normalization.
The form factor at zero-recoil that the FLAG 2019 review group [67] uses for their V_{cb} determination from $\bar{B} \to D^{*+} \ell^- \bar{\nu_\ell}$ is dominated by lattice inputs from the Fermilab/MILC and HPQCD collaborations which are both based on MILC $F^{B \to D^*}(1)$ result calculated for the $\bar{B} \to D^{*+} \ell^- \bar{\nu_\ell}$ channel in the lattice unquenched $N_f = 2 + 1$ approximation [68].

$$F(1) = 0.906 \pm 0.004_{stat} \pm 0.012_{syst} \tag{21}$$

where the first error is statistical and the second error is the sum in quadrature of all systematic errors.

The form factor at zero-recoil that the HFLAV 2018 review group [55] uses for their V_{cb} determination from $\bar{B} \to D^+ \ell^- \bar{\nu_\ell}$, $G^{B \to D}(1)$, is produced by the MILC collaboration [69].

$$G(1) = 1.0541 \pm 0.004_{stat} \pm 0.008_{syst} \tag{22}$$

[1] Note that HQE is not the same as HQET introduced in the theory section. HQET is used for extrapolations of heavy quark masses in lattice QCD calculations of exclusive determinations, whilst HQE is used for expressing inclusive quantities as a double expansion using the high mass of heavy quarks.

Ref. [69] has been able to reduce the uncertainty of the zero-recoil form factor due to the use of a much larger data set with several lattice spacing and lighter pions. For this result, ref. [69] has also included the heavy quark discretization error to the systematic error estimate, which makes the result more accurate.

7.1.2 Parameterizations

FLAG uses the BGL parameterization while HFLAV uses the CLN parameterization for their V_{cb} determinations. Both the BGL and the CLN parameterization are based on the same unitarity constraints but differ in that CLN employs HQET relations to reduce the number of parameters. [70] This means that CLN only needs four independent fit parameters, $\eta_{EW}F(1)|V_{cb}|$, ρ^2 and the form factor ratios R_1 and R_2, to describe the system, while BGL needs more parameters for the fit. [23, 26]
By using a fit of these form factor parameters, the results from the decay can be extrapolated to the zero-recoil point, where the normalization form factor, $F(1)$ or $G(1)$, from LQCD and the η_{EW} can be used to calculate the value of V_{cb} from $\eta_{EW}F(1)|V_{cb}|$ [21]. [55, 71]

7.1.3 Updated exclusive V_{cb}

It seems that the BGL and the CLN parameterizations used to determine the exclusive V_{cb} value are compatible with each other, as could be observed in figure 14. There is however a clear difference in uncertainty and still no full consensus about the use of parameterization.
In this thesis, the HFLAV average from 2021 [72] using the CLN parameterization is chosen as the updated exclusive V_{cb} value, since this HLFAV average is obtained from a combined fit of exclusive V_{ub} and V_{cb} measurements. This allows for inputs from $|V_{ub}|/|V_{cb}|$ measurements from LHCb, which provide extra input compared to only V_{cb} inputs. This combined fit can be observed in figure 15.

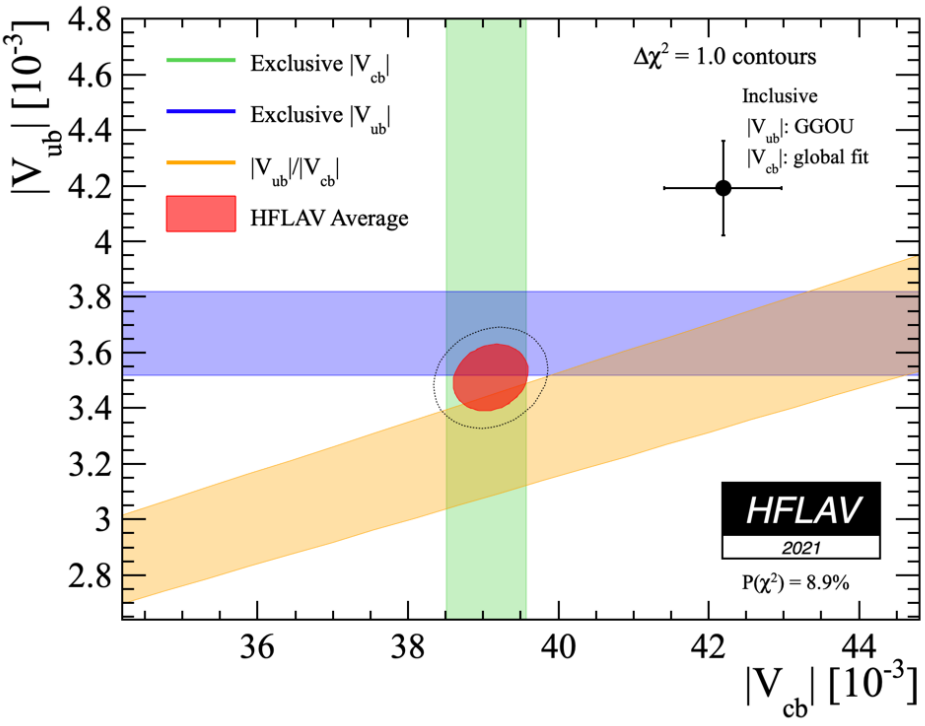

Figure 15: Combined exclusive $|V_{ub}|$ and $|V_{cb}|$ determination, 2021 HFLAV. For comparison, the inclusively determined V_{cb} value from the global fit, 42.19 ± 0.78, is also indicated with its respective error bars at the top right of the figure. [73]

The result of this combined fit for $|V_{cb}|$ is found to be the value (23), which is used as the updated exclusively determined V_{cb} value.

$$|V_{cb}| = (39.10 \pm 0.50) \times 10^{-3} \tag{23}$$

7.1.4 Numerical overview exclusive V_{cb}

Exclusive V_{cb}	Value	Error	Parameterization	Reference
Amhis et al.	39.09×10^{-3}	0.68×10^{-3}	BGL	FLAG [67]
Fleischer et al.	39.58×10^{-3}	1.17×10^{-3}	CLN	HFLAV [55]
Updated	39.10×10^{-3}	0.50×10^{-3}	CLN	HFLAV [72]

7.2 Inclusive determination

The disadvantage of exclusive determination is that the final hadronic state has to be taken into account, which brings extra uncertainty. Therefore, it is also important to look at the inclusive determination of $|V_{cb}|$.
Ref. [7] computes the branching fraction of $B_c^+ \to \tau^+\nu_\tau$ using an inclusively determined value, value (8), from the CKMfitter group as of summer 2019 [74]. This group has determined the V_{cb} value from a global fit. For inclusive determinations, this fit is performed using input from only inclusive quantities.

7.2.1 Updated inclusive V_{cb}

A recent paper, ref. [75], has determined an updated value, (24), for the inclusively reconstructed V_{cb}. In (25), the errors are separated into theoretical uncertainty, experimental uncertainty and the error due to uncertainty in the total semileptonic decay width. This paper has been able to reduce the uncertainty, because of a better control of higher order effects and improved determinations of the heavy quark masses [75].

$$|V_{cb}| = (42.16 \pm 0.51) \times 10^{-3} \tag{24}$$

$$|V_{cb}| = (42.16 \pm 0.30_{th} \pm 0.32_{exp} \pm 0.25_{\Gamma}) \times 10^{-3} \tag{25}$$

The dominant uncertainty that remains for this inclusive V_{cb} value, (25), comes from the experimental uncertainty, which comes from the error associated with the determination of the moments of the lepton energy and of the semileptonic branching fraction.

7.2.2 Numerical overview inclusive V_{cb}

Inclusive V_{cb}	Value	Error	Reference
Fleischer et al.	41.62×10^{-3}	0.80×10^{-3}	[74]
Updated	42.16×10^{-3}	0.51×10^{-3}	[75]

7.3 Prospects for future V_{cb} results

In the future, better results for both exclusive and inclusive reconstructions of V_{cb} are expected from Belle 2. For exclusive analyses, Belle 2 will be able to help in better understanding the form factors of $B \to D^*\ell\nu_\ell$ decays and reduce the relevant systematic uncertainties. For inclusive analyses, Belle 2 will try to improve the experimental determinations of the moments of lepton energy (kinetic moments) and semileptonic branching fraction of the $B \to X_c\ell\nu_\ell$ decays [76]. This will reduce the experimental uncertainty of (25) and therefore give a more accurate inclusively determined V_{cb}. It is furthermore possible to use other observables of $B \to X_c\ell\nu_\ell$ decays to measure the non-perturbative parameters used for HQE. Furthermore, from the theory side, the uncertainty of V_{cb} can be further reduced by investigating even more higher order effects [75].

8 Updated Standard Model prediction

8.1 Updated f_{B_c} and V_{cb}

For my update of the branching fraction, I have chosen the f_{B_c} value $f_{B_c} = (0.427 \pm 0.006) \times 10^{-3}$ GeV, which is the value from the HPQCD 2012 article [60] using the HISQ-HISQ formulation. This value is chosen as the updated value in anticipation of new, more accurate, f_{B_c} calculations using the HISQ-HISQ formulation in the future.

For the V_{cb} value, I have chosen to divide the update into an exclusive and an inclusive update, since these determinations continue to give conflicting results and there are no clear reasons to prefer one over the other.
The V_{cb} exclusively determined value was chosen to be updated to $|V_{cb}|_{excl.} = (39.10 \pm 0.50) \times 10^{-3}$, which is the HFLAV 2021 average [72]. This value is chosen as the updated value since this value was obtained from a combined fit including $|V_{ub}|/|V_{cb}|$ measurements, which provide extra input to the average.
The inclusively determined value was chosen to be updated to $|V_{cb}|_{incl.} = (42.16 \pm 0.51) \times 10^{-3}$, which is a value computed by [75]. This value is chosen as the updated value since this value was produced with a better control of higher order effects and improved determinations of the heavy quark mass.

8.2 Updated error analysis

The uncertainties accompanying the updated parameters can be visualized in the same figures as the analyzed starting parameters. The updated error analysis of the relative errors per parameter can be observed in figure 16.

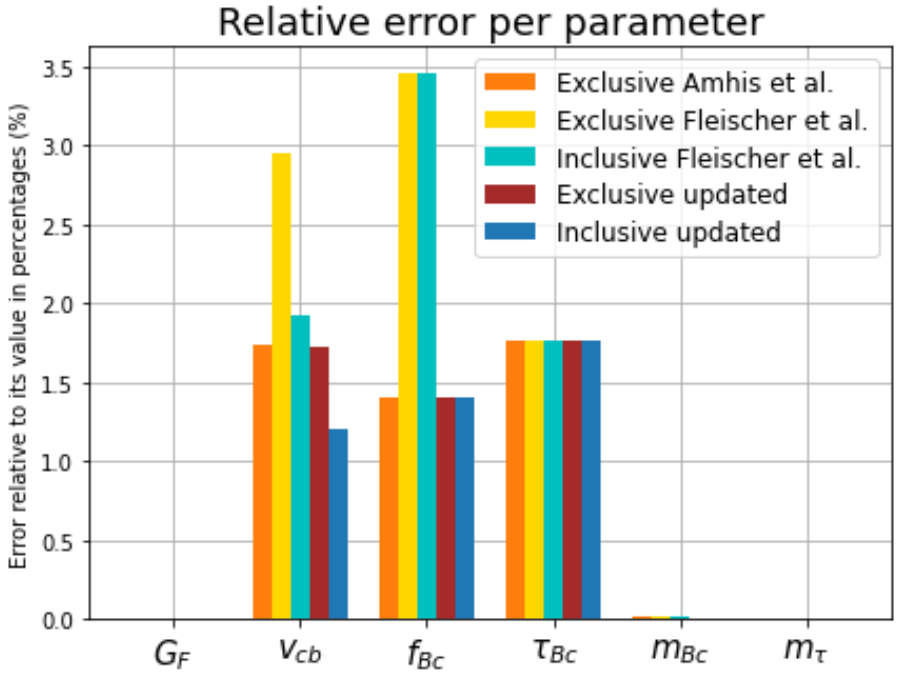

Figure 16: Relative errors of the parameters of the updated branching fraction prediction, compared with the relative errors of parameters of the investigated branching fraction predictions.

From this figure, it can be observed that the uncertainties of the V_{cb} exclusive and inclusive values and of the f_{B_c} values were all reduced. The error percentages of the V_{cb} and f_{B_c} are now approximately on the same level as the error percentage of the τ_{B_c}, around 1.5%. So, none of the parameters have a disproportionate uncertainty percentage. This means that work has to be performed on all three parameters, f_{B_c}, V_{cb} and τ_{B_c}, to further reduce the error of the branching fraction to make the SM prediction as accurate as possible.

The parameter errors can furthermore be represented as pie plots for the exclusive and inclusive updated predictions in 17, which visualize the error contribution of each parameter to total the branching fraction error.

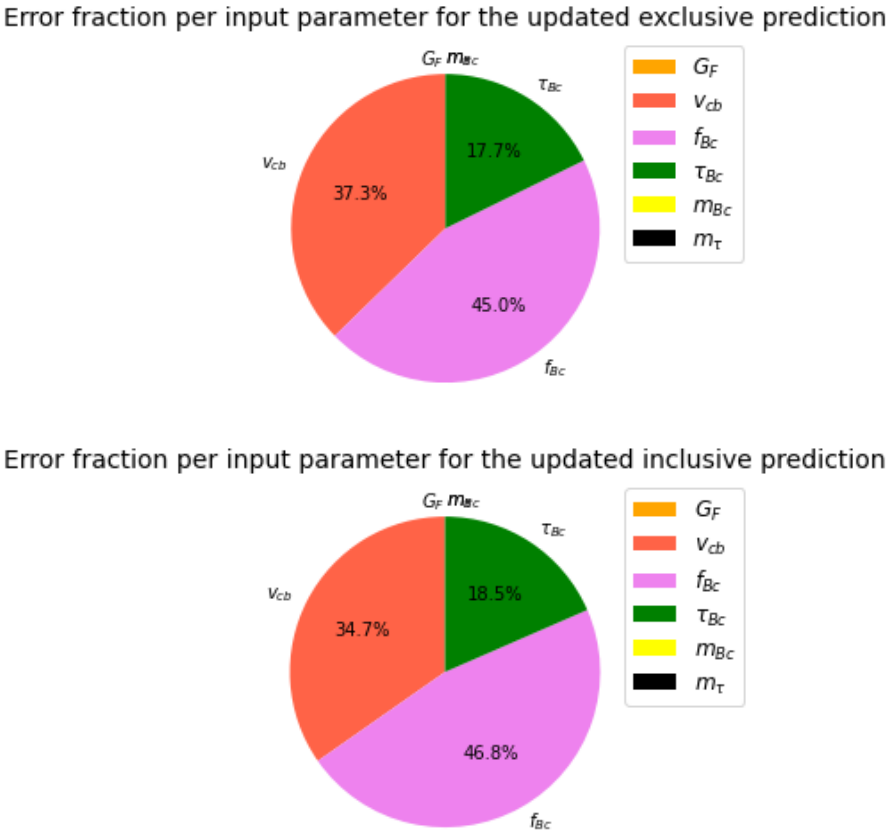

Figure 17: The error contribution of each parameter is expressed as a percentage of the total branching fraction error for the updated exclusive and inclusive predictions.

In the pie plots of 17, there is again confirmation of the parameter errors having a more equal representation in the total branching fraction error. There is however still a clear over-representation of the f_{B_c} and V_{cb} errors in the branching fraction error due to their quadratic representation in formula (3).

8.3 Updated branching fraction

After combining all the found updated values into the formula for the branching fraction, the following numerical values for the exclusively and inclusively determined branching fraction $B_c^+ \to \tau^+\nu_\tau$ are obtained:

$$\mathcal{B}(B_c^+ \to \tau^+\nu_\tau)^{SM}_{excl.} = (1.96 \pm 0.09) \times 10^{-2} \tag{26}$$

$$\mathcal{B}(B_c^+ \to \tau^+\nu_\tau)^{SM}_{incl.} = (2.28 \pm 0.10) \times 10^{-2} \tag{27}$$

The uncertainty of the updated exclusive prediction is equivalent with the uncertainty of the state-of-the-art exclusive prediction. The uncertainty of the inclusive prediction is about twice as low as the prediction that was used as a reference.

9 Conclusion

In this thesis, I discussed the state-of-the-art SM predictions for the branching fraction of the decay $B_c^+ \to \tau^+ \nu_\tau$ and updated the numerical predictions with the latest inputs for f_{B_c} and V_{cb}, which were found to be the parameters with the biggest contribution to the uncertainty of the branching fraction.

For f_{B_c}, the meson decay constant, the method of discretizing the heavy bottom quark onto the QCD lattice for calculations turned out to be an important factor. Two different methods, namely HISQ and NRQCD, are being used in the field. The HISQ formulation was chosen as the method that should provide the updated f_{B_c} value in anticipation of new, more accurate, f_{B_c} computations using this formulation. I anticipate this based on recently published updated results for most other D- and B-meson decay constants.

For the V_{cb} parameter, the main focus of the investigation was on the difference between exclusive and inclusive determinations and the different methods, involving different parameterizations, for obtaining exclusive V_{cb} determinations.
From the investigation of exclusive and inclusive determinations of V_{cb}, no clear reason was found to prefer one determination over the other. The V_{cb} value is therefore updated separately for exclusive and inclusive determinations.
The different parameterizations possible for exclusive determinations, the BGL and CLN parameterization, are thought to be compatible with each other. There is however no full consensus about the use of parameterization. Therefore, the updated exclusive V_{cb} value was not chosen based on the use of a specific parameterization, but based on obtaining the V_{cb} value from a combined fit of V_{cb} and V_{ub} data. This combined fit allows for extra $|V_{ub}|/|V_{cb}|$ input to obtain the exclusive V_{cb} result.
The updated inclusive V_{cb} value was chosen based on a reduction in uncertainty.

The updated exclusively determined prediction for the branching fraction $B_c^+ \to \tau^+ \nu_\tau$ is found to be $(1.96 \pm 0.09) \times 10^{-2}$. The uncertainty of this exclusive prediction is equivalent with the uncertainty of the state-of-the-art exclusive prediction. The updated inclusively determined prediction for the branching fraction $B_c^+ \to \tau^+ \nu_\tau$ is found to be $(2.28 \pm 0.10) \times 10^{-2}$. The uncertainty of the inclusive prediction is about twice as low as the prediction that was used as a reference.
Therefore, the updated predictions should provide an improved prediction of the numerical value of the branching fraction for the decay $B_c^+ \to \tau^+ \nu_\tau$, that can be used as reference for future comparison to the experimental measurement of this branching fraction.

References

[1] CERN, *Dark matter*, https://home.cern/science/physics/dark-matter.

[2] S. J. Ling, J. Sanny, and W. Moebs, *University Physics Volume 3*, Pearson, 2006.

[3] CERN, *The lhcb detector*, https://lhcb-outreach.web.cern.ch/detector/.

[4] LHCb, A. Buonaura, *Tests of lepton flavour universality at LHCb*, J. Phys. Conf. Ser. **1586** (2020) 012031.

[5] LHCb, G. Ciezarek, *$r(d^*)$ and $r(d)$ with $\tau^- \to \mu^-\nu_\tau\bar{\nu_\mu}$*, https://indico.cern.ch/event/1187939/attachments/2530158/4355180/DTaunu_CERNSeminar.pdf, 2022.

[6] Y. Amhis *et al.*, *Prospects for $B_c^+ \to \tau^+\nu$ at FCC-ee*, JHEP **12** (2021) 133, arXiv:2105.13330.

[7] R. Fleischer, R. Jaarsma, and G. Tetlalmatzi-Xolocotzi, *Mapping out the space for new physics with leptonic and semileptonic $B_{(c)}$ decays*, Eur. Phys. J. C **81** (2021) 658, arXiv:2104.04023.

[8] J. Arnau Romeu, *Recherche des désintégrations violant la saveur leptonique Bs -> tμ et Bd -> tμ avec l'expérience LHCb*, theses, Aix Marseille Université, 2018.

[9] CERN, *The standard model*, https://home.cern/science/physics/standard-model.

[10] M. Kobayashi and T. Maskawa, *CP Violation in the Renormalizable Theory of Weak Interaction*, Prog. Theor. Phys. **49** (1973) 652.

[11] B. R. Martin and G. Shaw, *Particle Physics*, John Wiley and Sons Ltd., 3 ed., 2008.

[12] LHCb, CMS, ATLAS, L. Anderlini, *Properties and Decays of the B_c^+ meson*, in *12th Conference on Flavor Physics and CP Violation*, 2014, arXiv:1407.8066.

[13] Z.-J. Xiao and X. Liu, *The two-body hadronic decays of B_c meson in the perturbative QCD approach: A short review*, Chin. Sci. Bull. **59** (2014) 3748, arXiv:1401.0151.

[14] *The CKM matrix and the unitarity triangle. Workshop, CERN, Geneva, Switzerland, 13-16 Feb 2002: Proceedings*, CERN Yellow Reports: Conference Proceedings, 2003. doi: 10.5170/CERN-2003-002-corr.

[15] CKMfitter group, *Results ckmfitter as of spring 2021.*, http://ckmfitter.in2p3.fr/www/results/plots_spring21/ckm_res_spring21.html#etiquette1.

[16] CKMfitter Group, J. Charles *et al.*, *CP violation and the CKM matrix: Assessing the impact of the asymmetric B factories*, Eur. Phys. J. C **41** (2005) 1, arXiv:hep-ph/0406184.

[17] Particle Data Group, R. L. Workman *et al.*, *Review of Particle Physics*, PTEP **2022** (2022) 083C01.

[18] A. J. Buras, *Unitarity triangle: 2002 and beyond*, in *14th Rencontres de Blois on Matter - Antimatter Asymmetry*, 2002, arXiv:hep-ph/0210291.

[19] M. Bona, *Flavour physics and cp violation*, https://indico.cern.ch/event/745783/contributions/3082096/attachments/1690117/2719220/bona_lecture2.pdf, 2018.

[20] G. Buchalla, *Heavy quark theory*, in *55th Scottish Universities Summer School in Physics: Heavy Flavor Physics (SUSSP 2001)*, 57–104, 2002, arXiv:hep-ph/0202092.

[21] J. Harrison, C. Davies, and M. Wingate, *$|V_{cb}|$ from the $\bar{B}^0 \to D^{*+}\ell^-\bar{\nu}$ zero-recoil form factor using $2+1+1$ flavour HISQ and NRQCD*, PoS **LATTICE2016** (2017) 287, arXiv:1612.06716.

[22] Fermilab Lattice, MILC, J. A. Bailey *et al.*, *Update of $|V_{cb}|$ from the $\bar{B} \to D^*\ell\bar{\nu}$ form factor at zero recoil with three-flavor lattice QCD*, Phys. Rev. D **89** (2014) 114504, arXiv:1403.0635.

[23] D. Bigi, P. Gambino, and S. Schacht, *A fresh look at the determination of $|V_{cb}|$ from $B \to D^* \ell \nu$*, Phys. Lett. B **769** (2017) 441, arXiv:1703.06124.

[24] Belle, R. Glattauer *et al.*, *Measurement of the decay $B \to D \ell \nu_\ell$ in fully reconstructed events and determination of the Cabibbo-Kobayashi-Maskawa matrix element $|V_{cb}|$*, Phys. Rev. D **93** (2016) 032006, arXiv:1510.03657.

[25] Belle, A. Abdesselam *et al.*, *Precise determination of the CKM matrix element $|V_{cb}|$ with $\bar{B}^0 \to D^{*+} \ell^- \bar{\nu}_\ell$ decays with hadronic tagging at Belle*, arXiv:1702.01521.

[26] B. Grinstein and A. Kobach, *Model-Independent Extraction of $|V_{cb}|$ from $\bar{B} \to D^* \ell \overline{\nu}$*, Phys. Lett. B **771** (2017) 359, arXiv:1703.08170.

[27] S. Jaiswal, S. Nandi, and S. K. Patra, *Extraction of $|V_{cb}|$ from $B \to D^{(*)} \ell \nu_\ell$ and the Standard Model predictions of $R(D^{(*)})$*, JHEP **12** (2017) 060, arXiv:1707.09977.

[28] Belle, E. Waheed *et al.*, *Measurement of the CKM matrix element $|V_{cb}|$ from $B^0 \to D^{*-} \ell^+ \nu_\ell$ at Belle*, Phys. Rev. D **100** (2019) 052007, arXiv:1809.03290, [Erratum: Phys.Rev.D 103, 079901 (2021)].

[29] Belle Collaboration, M. Huschle *et al.*, *Measurement of the branching ratio of $\overline{B} \to D^{(*)} \tau^- \overline{\nu}_\tau$ relative to $\overline{B} \to D^{(*)} \ell^- \overline{\nu}_\ell$ decays with hadronic tagging at belle*, Phys. Rev. D **92** (2015) 072014.

[30] Belle Collaboration, G. Caria *et al.*, *Measurement of $\mathcal{R}(d)$ and $\mathcal{R}(D^*)$ with a semileptonic tagging method*, Phys. Rev. Lett. **124** (2020) 161803.

[31] Belle Collaboration, S. Hirose *et al.*, *Measurement of the τ lepton polarization and $r(D^*)$ in the decay $\overline{B} \to D^* \tau^- \overline{\nu}_\tau$*, Phys. Rev. Lett. **118** (2017) 211801.

[32] BABAR Collaboration, J. P. Lees *et al.*, *Evidence for an excess of $\overline{B} \to D^{(*)} \tau^- \overline{\nu}_\tau$ decays*, Phys. Rev. Lett. **109** (2012) 101802.

[33] The BABAR Collaboration, J. P. Lees *et al.*, *Measurement of an excess of $\overline{B} \to D^{(*)} \tau^- \overline{\nu}_\tau$ decays and implications for charged higgs bosons*, Phys. Rev. D **88** (2013) 072012.

[34] LHCb, R. Aaij *et al.*, *Measurement of the ratio of branching fractions $\mathcal{B}(\bar{b}^0 \to D^{*+} \tau^- \overline{\nu}_\tau)/\mathcal{B}(\bar{b}^0 \to D^{*+} \mu^- \overline{\nu}_\mu)$*, Phys. Rev. Lett. **115** (2015) 111803.

[35] LHCb Collaboration, R. Aaij *et al.*, *Measurement of the ratio of the $B^0 \to D^{*-} \tau^+ \nu_\tau$ and $B^0 \to D^{*-} \mu^+ \nu_\mu$ branching fractions using three-prong τ-lepton decays*, Phys. Rev. Lett. **120** (2018) 171802.

[36] LHCb Collaboration, R. Aaij *et al.*, *Test of lepton flavor universality by the measurement of the $B^0 \to D^{*-} \tau^+ \nu_\tau$ branching fraction using three-prong τ decays*, Phys. Rev. D **97** (2018) 072013.

[37] MILC, A. Bazavov *et al.*, *Nonperturbative QCD Simulations with 2+1 Flavors of Improved Staggered Quarks*, Rev. Mod. Phys. **82** (2010) 1349, arXiv:0903.3598.

[38] D. Scheffler, *Two-Color Lattice QCD with Staggered Quarks*. Technical University Darmstadt, 2015.

[39] Particle Data Group, M. Tanabashi *et al.*, *Review of Particle Physics*, Phys. Rev. D **98** (2018) 030001.

[40] C. Davies, *Lattice QCD: A Guide for people who want results*, in *58th Scottish Universities Summer School in Physics (SUSSP58): A NATO Advanced Study Institute and EU Hadron Physics 13 Summer Institute*, 233–272, 2005, arXiv:hep-lat/0509046.

[41] H. B. Nielsen and M. Ninomiya, *A no-go theorem for regularizing chiral fermions*, Physics Letters B **105** (1981) 219.

[42] B. Assi and B. A. Kniehl, *Matching the Standard Model to HQET and NRQCD*, arXiv:2011.06447.

[43] HPQCD, UKQCD, E. Follana *et al.*, *Highly improved staggered quarks on the lattice, with applications to charm physics*, Phys. Rev. D **75** (2007) 054502, arXiv:hep-lat/0610092.

[44] J. F. Lagae and D. K. Sinclair, *Improved staggered quark actions with reduced flavor symmetry violations for lattice QCD*, Phys. Rev. D **59** (1999) 014511, arXiv:hep-lat/9806014.

[45] A. Bazavov *et al.*, *B- and D-meson leptonic decay constants from four-flavor lattice QCD*, Phys. Rev. D **98** (2018) 074512, arXiv:1712.09262.

[46] M. Neubert, *Heavy quark effective theory*, Subnucl. Ser. **34** (1997) 98, arXiv:hep-ph/9610266.

[47] P. Mohanta and S. Basak, *Construction of $bb\bar{u}\bar{d}$ tetraquark states on lattice with NRQCD bottom and HISQ up and down quarks*, Phys. Rev. D **102** (2020) 094516, arXiv:2008.11146.

[48] G. P. Lepage *et al.*, *Improved nonrelativistic qcd for heavy-quark physics*, Phys. Rev. D **46** (1992) 4052.

[49] C. Hughes, C. T. H. Davies, and C. J. Monahan, *New methods for B meson decay constants and form factors from lattice NRQCD*, Phys. Rev. D **97** (2018) 054509, arXiv:1711.09981.

[50] The University of North Carolina at Chapel Hill, Department of Physics and Astronomy, D. Deardorff, *Introduction to measurements and error analysis.*, https://users.physics.unc.edu/~deardorf/uncertainty/UNCguide.html, 2000.

[51] I. Farrance and R. Frenkel, *Uncertainty of Measurement: A Review of the Rules for Calculating Uncertainty Components through Functional Relationships.*, Clin Biochem Rev. **33** (2012) 49.

[52] R. J. H. Klein-Douwel, *Data and error analysis*, University of Groningen, 2013.

[53] University of Toronto, Department of Physics, D. M. Harrison, *Error analysis in experimental physical science*, https://faraday.physics.utoronto.ca/PVB/Harrison/ErrorAnalysis/Propagation.html, 2001.

[54] LHCb, R. Aaij *et al.*, *Precision measurement of the B_c^+ meson mass*, JHEP **07** (2020) 123, arXiv:2004.08163.

[55] HFLAV, Y. S. Amhis *et al.*, *Averages of b-hadron, c-hadron, and τ-lepton properties as of 2018*, Eur. Phys. J. C **81** (2021) 226, arXiv:1909.12524.

[56] LHCb, R. Aaij *et al.*, *Measurement of the B_c^+ meson lifetime using $B_c^+ \to J/\psi\mu^+\nu_\mu X$ decays*, Eur. Phys. J. C **74** (2014) 2839, arXiv:1401.6932.

[57] LHCb, R. Aaij *et al.*, *Measurement of the lifetime of the B_c^+ meson using the $B_c^+ \to J/\psi\pi^+$ decay mode*, Phys. Lett. B **742** (2015) 29, arXiv:1411.6899.

[58] J. L. Rosner and S. Stone, *Decay Constants of Charged Pseudoscalar Mesons*, arXiv:0802.1043.

[59] HPQCD, B. Colquhoun *et al.*, *B-meson decay constants: a more complete picture from full lattice QCD*, Phys. Rev. D **91** (2015) 114509, arXiv:1503.05762.

[60] C. McNeile *et al.*, *Heavy meson masses and decay constants from relativistic heavy quarks in full lattice QCD*, Phys. Rev. D **86** (2012) 074503, arXiv:1207.0994.

[61] C. Sun, R.-H. Ni, and M. Chen, *The Decay constants of $B_c(nS)$ and $B_c^*(nS)$*, arXiv:2209.06724.

[62] HPQCD, R. J. Dowdall *et al.*, *B-Meson Decay Constants from Improved Lattice Nonrelativistic QCD with Physical u, d, s, and c Quarks*, Phys. Rev. Lett. **110** (2013) 222003, arXiv:1302.2644.

[63] P. Gambino, *B semileptonic moments at NNLO*, JHEP **09** (2011) 055, arXiv:1107.3100.

[64] M. Fael, T. Mannel, and K. K. Vos, *The Heavy Quark Expansion for Inclusive Semileptonic Charm Decays Revisited*, JHEP **12** (2019) 067, arXiv:1910.05234.

[65] G. Ricciardi, *Theory: Semileptonic B Decays and $|V_{xb}|$ update*, PoS **BEAUTY2020** (2021) 031, arXiv:2103.06099.

[66] John Hopkins University, Department of Physics and Astronomy, A. F. Falk, *The heavy quark expansion of qcd*, https://inis.iaea.org/collection/NCLCollectionStore/_Public/30/040/30040454.pdf, 1996.

[67] Flavour Lattice Averaging Group, S. Aoki *et al.*, *FLAG Review 2019: Flavour Lattice Averaging Group (FLAG)*, Eur. Phys. J. C **80** (2020) 113, arXiv:1902.08191.

[68] Fermilab Lattice and MILC Collaborations, J. A. Bailey *et al.*, *Update of $|V_{cb}|$ from the $\overline{B} \to D^* \ell \overline{\nu}$ form factor at zero recoil with three-flavor lattice qcd*, Phys. Rev. D **89** (2014) 114504.

[69] MILC, J. A. Bailey *et al.*, *$B \to D \ell \nu$ form factors at nonzero recoil and $|V_{cb}|$ from 2+1-flavor lattice QCD*, Phys. Rev. D **92** (2015) 034506, arXiv:1503.07237.

[70] D. Bigi and P. Gambino, *Revisiting $B \to D \ell \nu$*, Phys. Rev. D **94** (2016) 094008, arXiv:1606.08030.

[71] D. Bigi and P. Gambino, *Revisiting $b \to d \ell \nu$*, Phys. Rev. D **94** (2016) 094008.

[72] HFLAV, Y. Amhis *et al.*, *Averages of b-hadron, c-hadron, and τ-lepton properties as of 2021*, arXiv:2206.07501.

[73] HFLAv, Y. Amhis *et al.*, *Updates of Semileptonic Results for the 2021 Average*, https://hflav-eos.web.cern.ch/hflav-eos/semi/spring21/html/ExclusiveVub/exclVubVcb.html, 2021.

[74] CKMfitter group, J. Charles, *Results ckmfitter as of summer 2019.*, http://ckmfitter.in2p3.fr/www/results/plots_summer19/num/ckmEval_results_summer19.html.

[75] M. Bordone, B. Capdevila, and P. Gambino, *Three loop calculations and inclusive Vcb*, Phys. Lett. B **822** (2021) 136679, arXiv:2107.00604.

[76] Belle-II, L. Aggarwal *et al.*, *Snowmass White Paper: Belle II physics reach and plans for the next decade and beyond*, arXiv:2207.06307.